Chapter 2

Chronology and stratigraphy of the valley systems

Chris O. Hunt, Michelle Farrell, Katrin Fenech, Charles French, Rowan McLaughlin, Maarten Blaauw, Jeremy Bennett, Rory P. Flood, Sean D. F. Pyne-O'Donnell, Paula J. Reimer, Alastair Ruffell, Alan J. Cresswell, Timothy C. Kinnaird, David Sanderson, Sean Taylor, Caroline Malone, Simon Stoddart & Nicholas C. Vella

2.1. Methods for dating environmental and climate change in the Maltese Islands

Rowan McLaughlin, Maarten Blaauw, Rory P. Flood, Charles French, Chris O. Hunt, Michelle Farrell, Katrin Fenech, Sean D.F. Pyne-O'Donnell, Alan J. Cresswell, David C.W. Sanderson, Timothy C. Kinnaird, Paula J. Reimer & Nicholas C. Vella

Adequate absolute dating is critical to understanding the past, especially where data concerning environmental changes from different sites are being compared, as chronology is often the only reliable way to compare evidence from multiple contexts. The archaeological chronology of Malta is becoming increasingly well resolved and this sets up a challenge – how can we obtain comparable high-resolution chronologies of environmental change in the Maltese Islands? The Maltese landforms pose significant barriers to achieving this goal, as much of the available palaeoenvironmental evidence is limited to cores in alluvial or shallow-marine sediments, which contain materials that have been subject to much re-working through time. In this chapter, we introduce and discuss the various techniques that the *FRAGSUS Project* has brought to bear on this problem, and review the main approaches used.

2.1.1. Data sources for chronology building

2.1.1.1. Background: the cultural sequence of Malta

Rowan McLaughlin

A key aim of the *FRAGSUS Project* has been to establish the parameters that define the relationships between people and their environment in restricted island settings. The human story of Malta and the timing of its unparalleled cultural developments are therefore of great interest, as the focus of our work is on the synchronization of data from palaeoecological and archaeological investigations. Therefore, in parallel with detailed investigation of the palaeoenvironment, the *FRAGSUS Project* conducted archaeological excavations that have re-dated the cultural sequence on the islands. Details of this work are given in detail in Volume 2 and summarized here and in Tables 2.1–2.6.

2.1.1.2. Radiocarbon dating

Rowan McLaughlin, Paula J. Reimer & Maarten Blauuw

Radiocarbon dating provided many of the fundamental data that underpin the chronologies discussed by the *FRAGSUS Project*. Radiocarbon is a well-established technique that estimates the age of once-living things by measuring the quantity of naturally radioactive carbon in a sample (Bronk Ramsey 2008b). Samples suitable for radiocarbon dating include charcoal, seeds, bones and the decayed organic fraction of soil (or humus). For the *FRAGSUS Project*, radiocarbon dating was carried out using accelerator mass spectrometry (AMS) at the ^{14}CHRONO Centre, Queen's University Belfast, using protocols described by Reimer *et al.* (2015). The samples all derived from material either picked out of the sediment cores during their processing for pollen and molluscan analyses described in Chapters 3 and 4, or through sieving 'core catcher' samples – material at the bottom of each core section removed from the profile during extraction of each sediment core segment and bagged separately.

As discussed in detail below, the radiocarbon dates were used to build a chronology (Figs. 2.1 & 2.2) – a time-scale against which other data could be plotted, such as the changing patterns of vegetation revealed in the pollen studies. This was not a simple undertaking, as alluvial sediments in Malta were originally deposited during relatively high-energy rainstorms, causing much recycling of organic material and thus radiocarbon results that may not necessarily truly reflect the date they were buried. In the case of the sediment cores studied by the *FRAGSUS Project*, as described below, this was done using Bayesian age-depth modelling techniques (Blaauw & Christen 2011).

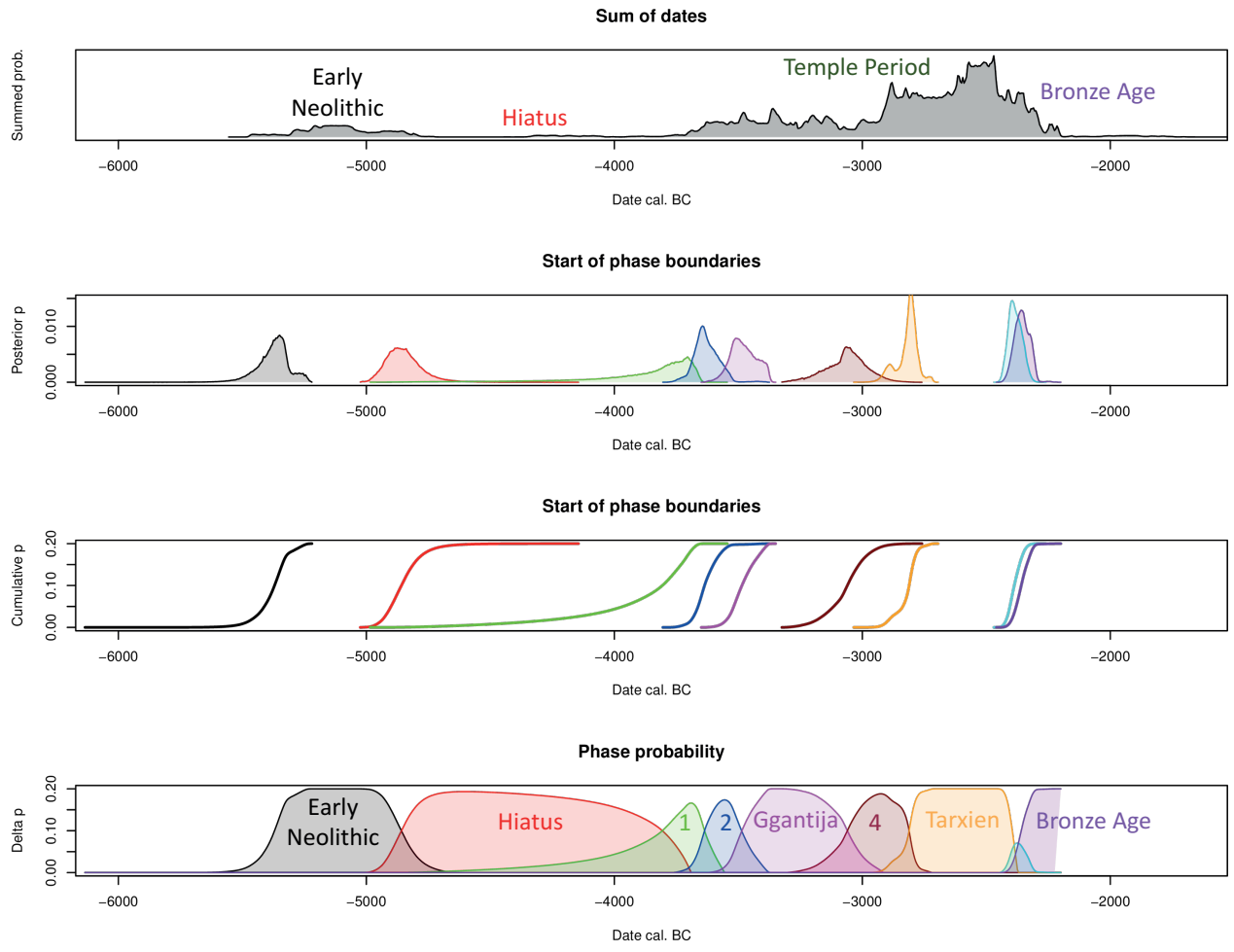

Figure 2.1. *Summary of new radiocarbon dating of Neolithic and Bronze Age sites on Gozo and Malta (R. McLaughlin).*

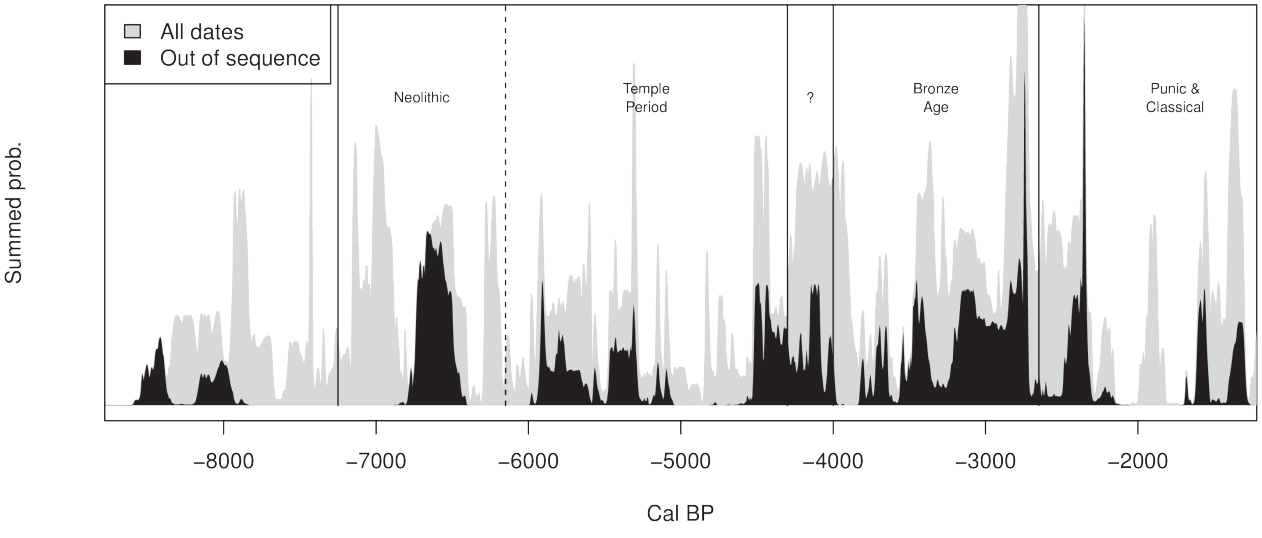

Figure 2.2. *Summed radiocarbon ages for the sediment cores on Gozo and Malta (R. McLaughlin).*

Table 2.1. *The cultural sequence of the Maltese Islands (with all dates calibrated).*

Period & events	From	To	Cultural development
No certain human impact	8000 BC	6000 BC	Impact of major climate events on vegetation
Possible early Neolithic farming: Għar Dalam	6000 BC	5400 BC	Palynological evidence for cereal cultivation and grazing
Early Neolithic: Skorba	5400 BC	4800 BC	Agriculture and permanent settlement, cereal farming, with a peak at 4800 BC, livestock, pottery manufacture; distinctive 'Skorba' material culture
Fifth millennium BC hiatus	4800 BC	3800 BC	Much reduced archaeological evidence, but environmental evidence for agriculture
Temple Period: Żebbuġ phase	3800 BC	3600 BC	'Resettlement' and early megaliths; very high levels of pottery manufacture; burials in rock-cut tombs
Temple Period: Mġarr phase	3600 BC	3400 BC	Change in material culture style
Temple Period: Ġgantija phase	3400 BC	2900 BC	Elaboration of megalithic architecture; change in material culture
Temple Period: Saflieni phase	2900 BC	2850 BC	Elaboration of burial practices
Temple Period: Tarxien phase	2850 BC	2400 BC	Further architectural and ritualistic elaboration; fluorescence of figurative art and other forms of material culture
Thermi ware	2400 BC	2200 BC	An attenuated continuation of Tarxien culture, but with new, imported, pottery forms
Third millennium hiatus	2200 BC	2000 BC	Third millennium hiatus
Earlier Bronze Age (Tarxien Cemetery)	2000 BC	1500 BC	Sudden change in burial practice, megalithic buildings no longer elaborated upon, general reduction in activity, hiatus in cereal agriculture, widespread livestock grazing and eventual agricultural re-intensification
Later Bronze Age	1500 BC	750 BC	Full return of cereal farming; hilltop settlement
Phoenician/Punic	750 BC	218 BC	New cultural and religious developments; viticulture; olive cultivation from the late Punic period; wider trade networks
Roman/Byzantine	218 BC	AD 870	Urban growth; intensive viticulture; internationalization
Arab/Norman	AD 870	AD 1530	Immigration; changing practices of agriculture and irrigation; introduction of the Semitic language; fortifications
Knights	AD 1530	AD 1798	New wave of urban developments; refortification
Modern	AD 1798	present	Growing population density; eventual abandonment of livestock herding; intensive horticulture; industrialization

Radiocarbon dating was also used to investigate directly some aspects of the changing ecology of the islands, following closely the methods of Hill *et al*. (2017). In this exercise, the differences between the carbon ecology of the past and the present were studied by measuring the radiocarbon content of modern snail shells, and comparing the results with snail shells of a known age, removed from an archaeological context at the Taċ-Ċawla settlement using data embedded in the shells of snails removed from an archaeological context of known age and AMS dated.

2.1.1.3. Optically stimulated luminescence (OSL) dating
Alan Cresswell, David C.W. Sanderson & Timothy C. Kinnaird

Luminescence dating estimates the time elapsed since material was heated or exposed to light. In the case of Optically Stimulated Luminescence (OSL) dating, quartz grains are used to estimate the age a sediment was buried. Although the limestone geology of the Maltese Islands is not naturally rich in quartz, windblown fine to very fine quartz sands from the Sahara deliver small quantities of silicates to the island, which are well suited to OSL dating. The *FRAGSUS Project* used OSL dating to provide a temporal framework to underpin investigations into the early Holocene topography of the Ramla and Marsalforn valleys on Gozo, and the excavations at the Neolithic temple sites of Ġgantija on Gozo and Skorba on Malta.

The study reported here uses luminescence techniques to develop chronological frameworks for these investigations. Chronologies have previously been developed based on radiocarbon analysis (Trump 1966; Renfrew 1972) for the temple complex at Skorba with calibrated dates ranging from *c*. 5000 to 3200 BC, however luminescence approaches have not been widely used on Malta and Gozo to date. Luminescence techniques have, however, been widely used in Neolithic contexts in the Mediterranean, and beyond, for establishing robust chronologies. Examples in the Mediterranean region include megalithic tombs at Cabeço dos Pendentes in Portugal (Kinnaird *et al.*

2015), Neolithic monuments in Corsica (Sanderson *et al.* 2014), deltaic sediments associated with cultural activity from the Neolithic onwards on Crete (Zacharias *et al.* 2009), and Neolithic settlements, cemeteries and landscapes in Cyprus (Kinnaird *et al.* 2007, 2013). These techniques have also been used to investigate rates of soil erosion in Greece (Fuchs *et al*. 2004) using material largely devoid of quartz minerals, and river development in Crete (Macklin *et al.* 2010), where quartz minerals are derived from the local sandstone.

The geology of Malta is dominated by limestone (see Chapter 1), resulting in locally derived soils largely devoid of silicate minerals suitable for luminescence dating. However, wind-blown sands from the Sahara are believed to have delivered small quantities of silicates to the islands. The Sahara is the largest source of aeolian dust, accounting for approximately half of the total atmospheric mineral dust burden (Scheuvens *et al.* 2013), with dust from the Sahara deposited in south and central America, the Atlantic Ocean, Europe and the Mediterranean, India and sub-Saharan Africa over the last five million years. In the Western Mediterranean, the dominant source of dust is from the Sahara (Scheuvens *et al.* 2013). Dust emission is a complex relationship between wind and surface conditions. Generally, small particles (<70 μm) experience large inter-particle cohesive forces relative to aerodynamic forces acting on the particles, with aerodynamic forces becoming relatively larger with larger grain size. Thus, larger grains are mobilized first and follow ballistic curves with impacts on the ground mobilizing the smaller particles (Schepanski 2018). Alluvial sediments are very prone to wind erosion, with temporally varying erodibility as the most susceptible particles are removed from the sediment with refreshing of sediments during floods (Schepanski 2018). Thus, dust emission strongly reflects environmental conditions, being largest in dry periods. The transport distance strongly depends on residence time in the atmosphere; fine particles (<70 μm) are kept aloft by atmospheric turbulence for durations of weeks and can be transported thousands of kilometres, with larger particles generally being deposited within a day, although larger particles are occasionally found >1000 km from their source (Schepanski 2018). The typical red Mediterranean soils, or *terra rossa*, on limestone substrates found throughout this region are also common on Malta and Gozo. The silicate minerals in similar soils in Greece have been attributed to aeolian deposition of material blown from North Africa, although larger mineral grains in low-lying regions have been attributed to local beaches (MacLeod 1980; Mizota *et al.* 1988). Yaalon (1997) argues that aeolian dust from the Sahara contributes to all soils in the Mediterranean region, with up to 50 per cent of aeolian material in limestone derived soils. Micromorphological investigations conducted within the *FRAGSUS Project* have already shown the presence of sand-sized silicates within local soils and sediments (French *et al.* 2018) (and see Chapter 5).

Quartz grains from the Sahara are expected to be well suited to OSL dating, with a reputation for being bright (e.g. Bevan *et al.* 2013; Kinnaird *et al.* 2013; Mauz *et al.* 2009; Russell & Armitage 2012), but they may not be abundant. Fuchs *et al.* (2004) have shown that similar soils in Greece without abundant quartz can be accurately dated. The relative abundance of these grains may reflect climatic variations, and in particular changes in aridity in the Sahara which may alter the supply of grains, and prevailing wind directions and strengths affecting the transport of these grains to Malta. Although it is expected that aeolian grains will be bleached in transit, many of the grains in the soils will have been transported to the islands before incorporation in the soils, having been reworked from earlier soils. The aim of the OSL investigations reported here is to provide a temporal framework to underpin investigations into the earlier Holocene topography of the Ramla and Marsalforn valleys, Gozo, and on the excavations at the Neolithic temple sites of Ġgantija on Gozo and Skorba and Tal-Istabal on Malta. The objective of the field campaign was to retrieve samples from existing soil/sediment profiles in Gozo for OSL dating, and to sample the new test excavations at Ġgantija and Skorba for micromorphological analyses with associated physical characterization, radiocarbon and OSL dating.

On Gozo, three profiles were sampled: 1) a terrace/palaeosol sequence on the western edge of the Neolithic temple site of Ġgantija on the Xagħra plateau; 2) an alluvial/hillwash sequence in the lower Ramla valley, which separates the Xagħra plateau from the In-Nuffara plateau to the south; and 3) a terrace/hillwash sequence in the upper Marsalforn valley (Fig. 5.17). From the more extensive geoarchaeological fieldwork of French and Taylor (see Chapter 5), it is known that the plateaux are largely denuded of soil and vegetation (i.e. Holocene strata). The little that remains in terms of (Holocene) hillwash (colluvium) and alluvial deposits is concentrated on the lower slopes and in the lower parts of the topography, such as in the Ramla and Marsalforn valleys. The OSL investigations in the Ramla and Marsalforn valleys were undertaken with the aim of generating a chronology for the sequences of buried palaeosols, hillwash and alluvial deposits preserved there, and thus provide the means to reconstruct the earlier Holocene to recent development of the Gozo valley-scape. At Ġgantija, the objective was to provide a chronology for the buried soil sequence

located just off-site, in test pit 1, to establish the soil catena history for this part of Gozo.

On Malta, two sites were sampled: 1) the archaeological and palaeosol sequence associated with the Neolithic temple site of Skorba; and 2) a terrace/palaeosol sequence located at a development site with Punic-Roman archaeology present at Tal-Istabal, Qormi, on the outskirts of Valletta in Malta. Test excavations in 2016 on the western edge of the Skorba temple/settlement had revealed a 1.5 m deep sequence, within which three curvilinear stone walls of the Neolithic period effectively sealed *c*. 70 cm of soil accumulation. From fieldwork, it is suggested that the lower *c*. 50 cm of this soil was in fact a buried soil, albeit with the upper *c*. 20 cm probably being disturbed (in the past). The objective here was to provide a chronology for the buried soil sequence, and identify any correlations between the soil formation/properties and prehistoric activity at Skorba.

Field and laboratory profile measurements were conducted on 60 samples from seven sequences. All samples were first appraised using the SUERC portable OSL reader, following an interleaved sequence of system dark count (background), infrared stimulated luminescence (IRSL) and OSL, similar to that described by Sanderson and Murphy (2010). This method allows for the calculation of IRSL and OSL net signal intensities, depletion indices and IRSL:OSL ratios, which are then used to generate luminescence-depth profiles. The patterns in these data allow initial inferences and conjectures about trends or discontinuities in field profiles to be made, in combination with other initial observations of the sedimentology, which are used to refine further sampling. Subsequent laboratory profiling measurements confirmed the presence of quartz in prepared sediments with generally bright luminescence signals, and opened the way for Single Aliquot Regenerative (SAR) OSL dating of quartz fractions (Murray & Wintle 2000) from 12 tube samples collected from the five sites. Estimates of the cosmic dose rate were obtained using latitude and altitude specific dose rates for Malta (0.17 ± 0.01 mGy a^{-1}) with corrections for estimated depth of overburden using the method of Prescott and Hutton (1994).

At both the Ġgantija temple and Skorba temple/settlement, profile samples collected from below the modern agricultural soils showed photon counts and apparent doses that increased steadily with depth, indicating that these buried soils accumulated gradually without subsequent disturbance. The OSL equivalent dose measurements showed no significant variation between aliquots, again indicating that the quartz minerals had been zeroed prior to deposition without subsequent disturbance and allowing robust ages to be determined. For both these locations, the OSL dates for the bottom of the sequences indicating the onset of soil accumulation were consistent at 8560±630 BC (Ġgantija) and 8780±710 BC (Skorba). At Ġgantija the top of this buried soil gives a Bronze Age OSL date of 1140±250 BC, whereas the OSL date for the top of the buried soil at Skorba is 7760±560 BC, predating the known Neolithic activity at the site.

In both the Ramla and Marsalforn valleys, OSL investigations were conducted on sequences of buried palaeosols, hillwash and alluvial deposits. For the Marsalforn valley, the profile samples show a slight increase in photon counts and dose with depth, suggesting a gradual build-up of material. However, the OSL samples show evidence of multiple dose components, including high dose residuals, consistent with variations in light exposure during the reworking of soils. The upper sample could not be reliably dated, and the lower two samples generated the same age within uncertainties (1560±240 BC and 1480±340 BC). The Ramla Valley profiles are complex, showing relatively high photon counts in the upper samples decreasing with depth, and no clear trend in the apparent dose estimates. The OSL samples all show evidence of multiple dose components, including both high dose residuals and modern OSL dates in the nineteenth and early twentieth centuries AD.

The investigations reported here, and detailed in Table 2.2 and Appendix 2, are the first applications of luminescence techniques on these sites. Despite the local limestone geology not supplying abundant quantities of silicates to the soils and sediments at these sites, micromorphological studies (see Chapter 5) have already shown the presence of small quantities of silicate minerals. Both field and laboratory profiling measurements had indicated that these minerals carry measurable luminescence signals, with the OSL signals associated with quartz the most promising for dating. Although the quartz yields from the samples collected for OSL dating were limited, the signals from the quartz grains extracted were generally bright, in most cases providing sufficient signal to quantify the ages of the sampled sediments and soils. It is known that dust from the Sahara has been transported across the Mediterranean, and beyond, for approximately five million years (Schepanski 2018) and that this has most probably contributed to the soils on Malta and Gozo. The large signals observed from the quartz grains studied here are similar to those observed from Saharan sand, supporting that source for the silicates measured. This work has demonstrated that even in locations where the local geology is deficient in quartz, OSL measurements can be conducted using aeolian quartz from more distant sources. In locations where this primary aeolian mineral

Table 2.2. *Quartz OSL sediment ages from the Marsalforn (2917–2919) and Ramla (2921–2923) valleys, the Skorba temple/buried soil sequence (2925–2927) and the Tal-Istabal, Qormi, buried soil (2930) (Note: Dates in italics are poorly constrained due to low precision and large dispersion of equivalent doses determined by OSL analysis).*

Sample ID	SUTL no.	Depth /cm	Date	Archaeological significance
Marsalforn valley				
OSL1	2917	175–180	*760±920 BC*	Constrains the final period that the upper incipient soil in hillwash was exposed, phase 2
OSL2	2918	265–270	1560±240 BC	Constrains the final period that the lower incipient soil in hillwash was exposed, phase 1
OSL3	2919	320–330	1480±340 BC	Constrains the onset of hillwash accumulation, phase 1
Ramla valley				
OSL4	2921	15–20	*AD 1880±16*	Provides a temporal constraint on degradation of upper slope
OSL5	2922	62–66	AD 1850±12	Provide temporal constraints on periods of colluviation
OSL6	2923	103–106	*AD 1910±30*	
Ġgantija Temple				
OSL7	2914	78	1140±250 BC	Constrains the final period that the buried soil was exposed
OSL8	2915	92	8560±630 BC	Constrains onset of soil formation
Tal-Istabal, Qormi				
OSL9	2930	295–298	AD 1620±23	Constrains the burial of soil
Skorba Neolithic site				
OSL10	2925	118	7760±560 BC	Constrains the final period that the buried soil was exposed
OSL11	2926	128	8090±590 BC	Constrains the age of the buried land surface
OSL12	2927	145	8780±710 BC	Constrains onset of soil formation

input is preserved this should retain a palaeoclimatic signal combining aridity history in the Saharan source regions and wind patterns that move these minerals across the Mediterranean region.

For most of the samples collected from hillwash and alluvial deposits in valleys, the equivalent doses showed variations of a factor of two to three between aliquots, reflecting inhomogeneous or partial bleaching of the quartz grains in these samples. This suggests that the erosion and sediment transport processes resulting in these deposits did not expose the minerals to sufficient light to remove all the residual signals from burial in earlier sediments. This could be the result of bulk movement of sediment or the rapid erosion, movement and re-burial of the minerals. Although reliable dates were not always quantifiable, the data do provide information about the processes of formation for these deposits.

For the soils directly associated with the Ġgantija and Skorba temple sites the equivalent dose values did not show significant dispersion, suggesting that the quartz grains had been well zeroed prior to burial and that there has not been substantial disturbance since then. This allowed ages to be determined even from the small number of aliquots available. This has demonstrated that OSL dating provides valuable information, and should be applied in any further studies of these, and similar, monuments on Malta and Gozo.

2.1.1.4. Tephrochronology

Sean D.F. Pyne-O'Donnell

Tephrochronology is a technique that identifies layers in sediment cores that contain volcanic glass shards (*cryptotephra*) that derive from eruptions of known date. These layers or isochrons – age-equivalent horizons – can be very useful in matching data from different coring sites and they can greatly aid the interpretation of radiocarbon dates. At face value there is significant potential for this work in the Maltese Islands, given their central position in the Mediterranean, downwind from several active volcanoes. However, the nature of sedimentation on the islands causes severe difficulties, as the *cryptotephra* can be diluted beyond detectible limits by rapid sediment run-off and accumulation. Nonetheless, it was possible to study the tephrochronology of the Xemxija 1 core by extracting sub-samples – 'rangefinders' every 5–7 cm through the core, aside from the upper 1.24 m of overburden and unfavourable brecciated clays present between 6.55 and 7.8 m. *Cryptotephra* were extracted using stepped-centrifuge flotation (Blockley *et al*. 2005), and any rangefinders containing tephra concentrations likely to represent a layer (i.e. greater than background levels) were then examined again at 1 cm resolution to identify the precise stratigraphic position of the peak. Once this was done, individual shards were picked

from peaks by micromanipulator (Lane *et al*. 2014; Pyne-O'Donnell 2004) for WDS-EPMA microprobe geochemical analysis at the Tephra Analytical Unit (TAU), School of Geosciences, University of Edinburgh using a Cameca SX100 electron probe micro-analyser (accelerating voltage of 15 kV and a focused 3 μm beam diameter) (Haywood 2012). Rhyolitic (Lipari, ID 3506), with basaltic (BCR2g) secondary standards were used to test analytical consistency. These geochemical data were then compared to reference data to allow their classification and to identify the source eruptions (*cf*. Albert *et al*. 2012; Civetta *et al*. 1988; Le Bas *et al*. 1986; MacDonald 1974; Peccerillo & Taylor 1976 and references therein). Details of the two tephra horizons identified in the Xemxija 1 sequence are given in Table 2.3.

2.1.2. Pottery finds

Rowan McLaughlin

Human settlement of the Maltese Islands is richly associated with the production and use of pottery, much of which is highly distinctive, and can be dated on the basis of its appearance and study of its fabric, even from quite small fragments (Malone *et al*. 2009a; Malone & Stoddart 2000). A more detailed discussion can be followed in *FRAGSUS* Volume 2. Throughout time, broken pottery was added to field soil with other midden materials to improve fertility. Consequently sediment cores frequently contain small sherds, some of which are identifiable. In cases where this added meaningful information to the chronology, the known age ranges of the pottery types (i.e. the cultural phases in Table 2.1) were included in the age-depth model of the sediment core. Details of pottery sherds used in this way are given in Table 2.3.

2.2. Basin infill ground penetrating radar surveys

Alastair Ruffell, Chris O. Hunt, Jeremy Bennett, Rory P. Flood, Simon Stoddart & Caroline Malone

2.2.1. Rationale

Stratigraphic successions for palaeoenvironmental reconstruction from areas proximal to archaeological sites are required for penecontemporaneous reconstruction of proxy changes (Shackleton *et al*. 1984). For the Maltese Islands, identification of such successions presents a challenge, since the landscape is dominated by rock exposures and thin soils. However, the islands' position on the Libyan Shelf has resulted in late Miocene (~5 mya) uplift, generated by the continued collision of the African Plate to the south, with the Eurasian Plate to the north. This movement is confirmed by dated raised marine deposits (Pedley 2011). Periodically dry river valleys occur throughout the islands, sourced by *widien* in the hinterlands that have provided a sediment source for any accommodation space located downstream or offshore. As a consequence, depressions close to present-day sea level (usually river valleys) comprise flat, fertile plains, underneath which a sediment record may be preserved. Identification of these potential sites can be made by visual observation, but in order to target viable coring locations and extract sediment that may yield useful material for reconstructing past environments, geophysics was used as a basin visualization and prospection tool to aid in the location of the deep core sites for intensive sampling, further described below.

2.2.2. Geophysics for basin fill identification

A range of geophysical techniques can be useful for the imaging of sediment thickness from a few metres to tens of metres in palaeo-valleys. The following were considered for the *FRAGSUS* Maltese Islands surveys:

The gravity/microgravity method relies on a density change between the surrounding country rock and the sediment fill, which is likely in the rock-prone landscape of the Maltese Islands. The method is powerful and requires post-processing of data in order to remove other gravimetric influences (Bouger Anomalies).

Seismic/electroseismic techniques are the standard method of both deep (kilometres) and shallow (tens of metres) imaging of rock and sediment layers and are dependent on density changes in the medium (as with gravity, above). Seismic imaging uses soundwaves as as source, and thus requires a source (commonly percussion such as a hammer shock to the ground (shallow), a mechanical weight-drop, Buffalo Gun/ airgun, small detonation, or vibration).

Ground penetrating radar (or GPR) is similar to the seismic method, but uses radiowaves instead of vibrations as a signal source, and reacts to changes in the electrical makeup of the subsurface (polarization of molecules), termed the dielectric constant (Appendix 1). As such, an energy source is easier to obtain, but this results in less overall depth penetration and only works well in sand, freshwater and rock. Saline and clay-rich subsurface successions are not conducive to GPR surveying.

The Electrical Resistivity Imaging (or Tomography; ERI or ERT) method relies on subsurface changes in chemistry (as opposed to density in the gravity and seismic methods), but uses an electrical charge and its underground impedance (resistivity) or flow (conductivity) to generate an image. The technique works in many environments, but like seismic and gravity, takes time to gather results.

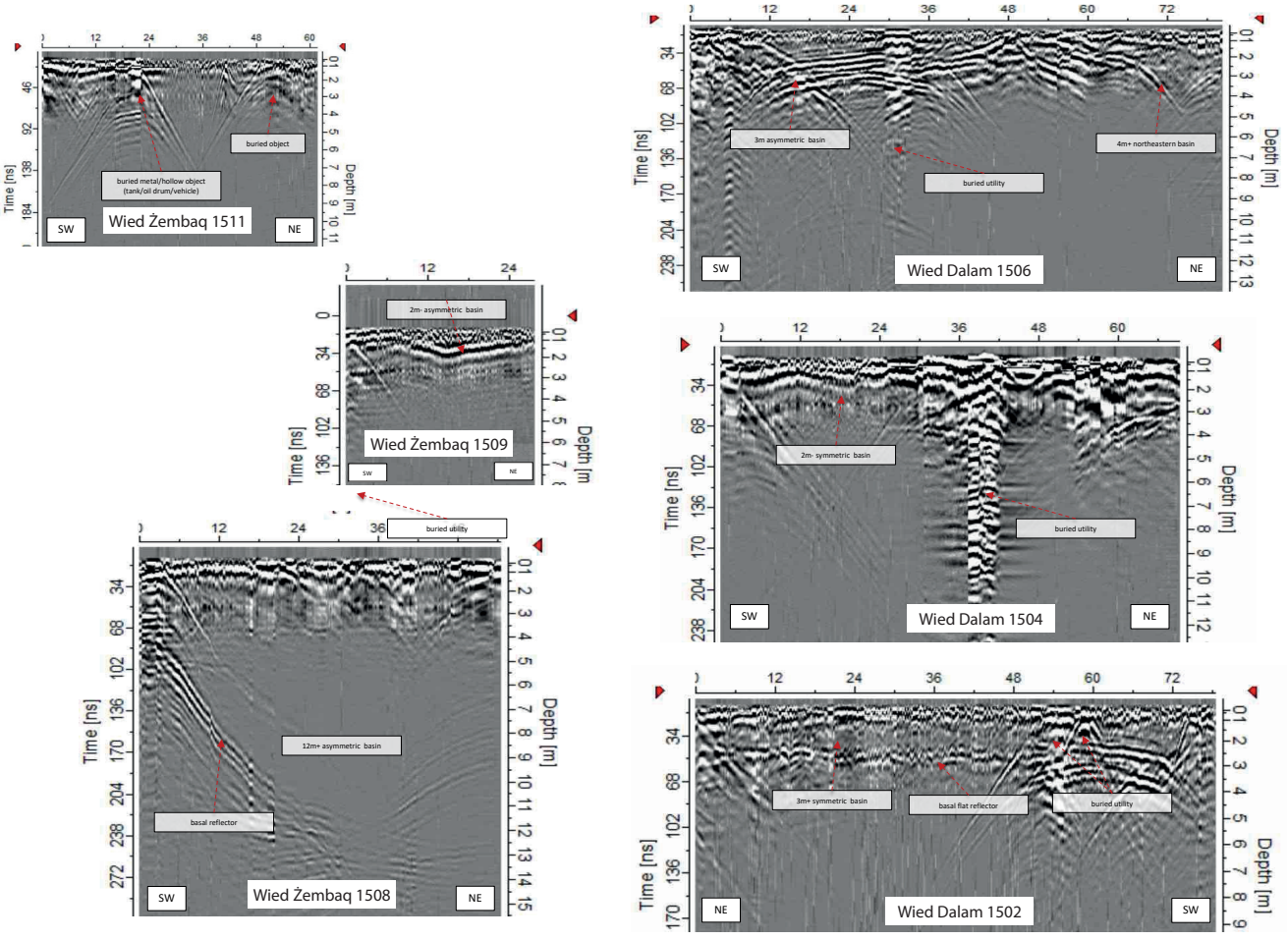

Figure 2.3. *The location of the Birżebbuġa Wied Dalam and Wied Żembaq basins and their GNSS-located GPR lines (A. Ruffell; image © 2020 Google).*

GPR was selected as the most rapid method available for the objective of identifying basin fills on Malta and Gozo. As a result of the limitations detailed above it was chosen as a reconnaissance method for valley fills selected by visual (field and orthophotography) methods, and the proximity of potential coring sites to prehistoric archaeological sites and previous coring/excavation investigations. ERI was also considered, but the success of GPR in identifying the majority of locations allowed coring to proceed without further assessment. The GPR system used was a Mala RAMAC system deploying 100 Mhz, 200 MHz, 250 Mhz antennas.

2.2.3. Valley locations

A. Birżebbuġa. This valley system includes a number of marine inlets, extending inland as plains: Wied Dalam, Wied Żembaq and Marsaxlokk. All three valleys were surveyed, but with poor results (particularly at Marsaxlokk because of the presence of the clay and saline soils). The locations of the Wied Dalam and Wied Żembaq basins and their GNSS-located GPR lines are shown in Figure 2.3. The Wied Dalam valley is underlain in some areas by two palaeo-valleys, of 3 and 4 m depth, and containing significant maritime and maritime-military utilities buried along the length of the valley. The Wied Żembaq valley is partly urbanized around a deep (15 m+) valley that thins to 2–3 m depth upstream (northwest) where fields occur and a coring location would be possible.

B. Marsalforn is a seaside location in the north of Malta and like Birżebbuġa, is urbanized. Likewise, the Marsalforn basin also has a thick sequence of deposits (10 m+) occurring closest to the sea (under the coast road), which thins inland to the west and south to 3–4 m under a flash-flood prone plain.

C. Xemxija. Similarly to the sites described above, the Xemxija valley meets the sea as a broad plain, but unlike the above, is wider and extends for some kilometres inland. The coastal area is urbanized, with extensive agriculture inland. The basin is 4–5 m deep at the coast, and this depth is maintained inland, where windmills have been replaced by mechanical water-pumps, attesting to the thick, permeable nature of the valley fill.

D. Mġarr ix-Xini. On the south coast of Gozo, this valley is of similar dimensions to Wied Żembaq, and to some extent, Wied Dalam, but is narrow and not urbanized. A 2–3 m deep basin occurs at the shore end to the southeast, this divides into two palaeo-valleys upstream to the northwest.

E. Low-lying, flat ground occurs southwest of Valletta Grand Harbour at Marsa, the location of a racecourse (hence it is flat, and likely underlain by significant quantities of sediment). GPR here was unsuccessful, possibly because the basin is too deep for imaging, and also filled with saline water, ingressed from the deep harbour. The soils may also be clay-rich and therefore less suitable for imaging. Thus Marsa, Marsaxlokk and two clay-filled dolines proved to be unsuccessful locations. A shallow, inland palaeovalley fill was also surveyed along Triq il-Mitħna-Triq Ġnien is-Sultan (southeast of Fontana, Gozo).

2.3. The sediment cores

Chris O. Hunt, Michelle Farrell, Rory P. Flood, Katrin Fenech, Rowan McLaughlin, Nicholas C. Vella, Sean Taylor & Charles French

2.3.1. Aims and methods

Investigation of the Holocene sequences addressed several issues:

1) There were suggestions from previous research (Carroll *et al.* 2012) that there were major discontinuities in sedimentation at some of the investigated localities. This is particularly marked at Marsa, where earlier Neolithic sediments are directly overlain by layers relating to the Punic and later periods, and at Salina Bay where Neolithic and Bronze Age sediments are overlain by sediments of likely nineteenth century date (Carroll *et al.* 2012, fig. 11).
2) There were indications from the existing research of spatial patterning of vegetation communities within the middle to late Holocene. For instance, Carroll *et al.* (2012) noted what appeared to be evidence for pine-dominated forest and Neolithic clearance at Marsa, contemporary with very open agricultural landscapes at Salina, while at Burmarrad, contemporary open grazed landscapes with lentisk scrub were reported (Djamali *et al.* 2013; Gambin *et al.* 2016). The number of palynological investigations of mid to late Holocene deposits available at the start of the *FRAGSUS Project* was insufficient to address adequately issues of spatial patterning of environments and vegetation, and hence land-use and human impact: critical for any evaluation of Neolithic sustainability and fragility, but also important for understanding the post-Neolithic development of the Maltese landscape.
3) Previous studies had not located early Holocene deposits which accumulated prior to the first Neolithic colonization, because they lay deeper

in the buried valley network than was reached by previous coring by Carroll *et al*. (2012) and Djamali *et al.* (2013). Therefore, deep boreholes were necessary to reach and sample the Early Holocene sediments.

4) Dating of cored sequences was an issue in previous research (Carroll *et al.* 2012; Djamali *et al*. 2013) with radiocarbon dates often falling out of stratigraphic order. This was likely the result of (1) recycling of old charcoal, and (2) intrusion of modern carbon through the coring process.

5) There has been remarkably little pollen-taphonomic work done in the Central Mediterranean countries. Pollen-vegetation relationships and patterns of pollen dispersal from different vegetation types are therefore unclear. This is a critical issue since some vegetation types, particularly maquis and garrigue, are dominated by insect-pollinated taxa. Further, some pollen assemblages reported by Carroll *et al.* (2012), Djamali *et al.* (2013) and Gambin *et al.* (2016) showed what could be interpreted as taphonomically biased features, such as high percentages of corrosion-resistant taxa such as *Pinus* and Lactuceae. These might result from differential preservation, recycling of pollen from soils, or losses during transport. Alternatively, these assemblages may reflect unbiased pollen assemblages derived from unusual ecologies.

The choice of coring sites was dictated by the prospect of obtaining partial sequences from each site that together would span the Holocene (Fig. 2.4). It was apparent from the earlier studies (e.g. Carroll *et al*. 2012; Djamali *et al*. 2013) that although sedimentation was discontinuous in each of the boreholes drilled by these researchers, the discontinuities occurred at different points in time. In times of sea level stand, sea level controlled sedimentation progrades seaward in wedge-shaped bodies, with increments deposited on the outer face of the wedge, and transport and reworking of fluvial deposits on the top of the sediment body by rivers. When sea level rises, deposition will migrate seaward if the sedimentation rate is greater than the rate of sea level rise, with deposition on the top of the sediment body and on its seaward face. On the other hand, sedimentation will be driven landward if there

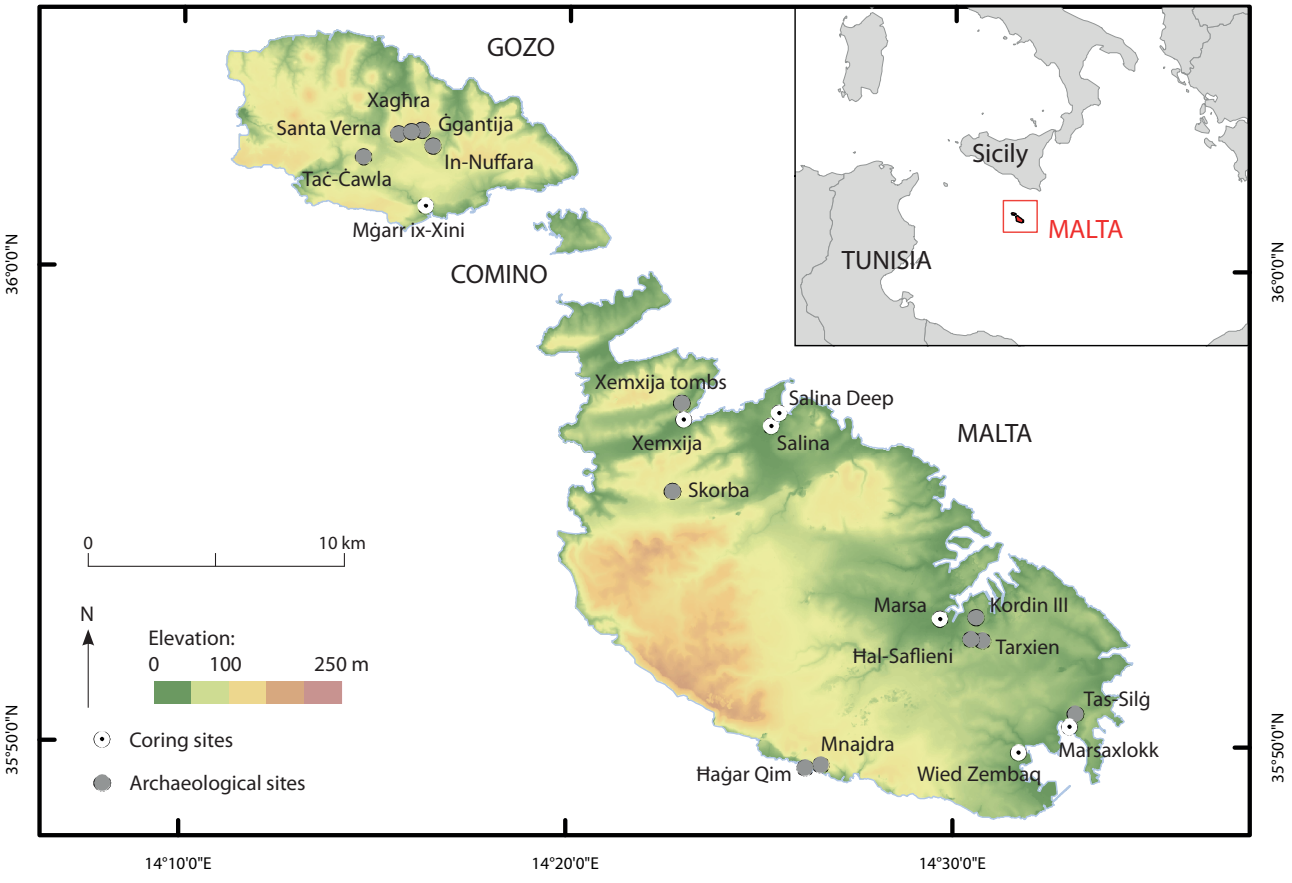

Figure 2.4. *The core locations in Malta and Gozo (R. McLaughlin).*

Table 2.3. *Dating results for positions in the sediment cores. The sites are Bahrija doline (BAH), Marsa Sports Ground (MARSA), Mellieħa Bay (MB), Mġarr ix-Xini (MGX), Marsaxlokk (MX), Salina Bay (SA), Salina Deep Core (SDC), Wied Żembaq (WZ) and Xemxija (XEM). Numbers following site codes denote different sequences recovered from the same site. (Note that tephra horizons are not definitive and pottery identifications are subjective).*

Core	D (cm)	Lab. ID	^{14}C date	±	F^{14}C	±	Calendar range (95%) BC/AD		Material
BAH1	49	UBA-30091	2195	29	.7609	.0028	-360	-180	Charcoal
MARSA2	275	UBA-29443	1487	34	.8310	.0035	430	650	Wood
MARSA2	335	UBA-29452	1510	32	.8287	.0033	430	640	Charcoal
MARSA2	375	UBA-29453	2687	35	.7157	.0031	-900	-800	Charcoal
MARSA2	395	UBA-29454	2686	35	.7158	.0031	-900	-800	Charcoal
MARSA2	435	UBA-29444	2584	28	.7250	.0026	-810	-600	Grape seed
MARSA2	455	UBA-29445	2357	42	.7458	.0039	-730	-360	*Fumaria* seed
MARSA2	475	UBA-29446	2754	41	.7098	.0036	-1000	-820	Seed
MARSA2	487	UBA-30605	7216	75	.4072	.0038	-6230	-5930	Charcoal
MARSA2	495	UBA-29447	3943	69	.6121	.0052	-2620	-2210	Plant macro
MARSA2	495	UBA-29455	3912	40	.6145	.0030	-2550	-2230	Charcoal
MARSA2	513	UBA-30606	2944	40	.6932	.0034	-1260	-1020	Charcoal
MARSA2	590	UBA-29448	2501	50	.7325	.0045	-790	-430	Seed
MARSA2	598	UBA-30607	2587	40	.7246	.0036	-830	-550	Charcoal
MARSA2	617	UBA-30608	2765	25	.7088	.0022	-980	-840	Charcoal
MARSA2	825	UBA-29451		1	1.0367	.0050			Insect
MB1	244	UBA-30092		1	1.0732	.0032			Wood
MGX1	54	UBA-29979		1	1.0138	.0079			Plant macro
MGX1	176	UBA-29980	1230	29	.8580	.0031	690	880	Wood
MGX1	239	UBA-29981	3443	31	.6514	.0025	-1880	-1660	Plant macro
MGX1	302	UBA-29982	2509	30	.7317	.0028	-790	-540	Plant macro
MGX1	365	UBA-29983	2466	30	.7356	.0028	-760	-430	Plant macro
MGX1	365	UBA-29984	2655	34	.7185	.0031	-890	-790	Charcoal
MGX1	428	UBA-29985	2998	35	.6885	.0030	-1380	-1120	Plant macro
MGX1	428	UBA-29986	6905	42	.4233	.0022	-5890	-5720	Wood
MGX1	554	UBA-29987	2991	40	.6891	.0034	-1390	-1060	Plant macro
MGX1	554	UBA-29988	2839	36	.7023	.0031	-1110	-910	Charcoal
MGX1	617	UBA-29989	3124	35	.6778	.0029	-1490	-1290	Plant macro
MGX1	695						-750	-250	Punic-period pot sherd
MGX1	702	UBA-33096	2339	33	.7474	.0031	-510	-360	Plant macro
MX1	86	UBA-29353	1567	29	.8228	.0030	420	560	Charcoal
MX1	186	UBA-29352	2354	33	.7460	.0031	-540	-380	Charcoal
MX1	286	UBA-29351	1444	51	.8355	.0053	440	670	Charcoal
MX1	386	UBA-29346	0	1	1.0397	.0031			Plant macro
MX2	200	UBA-29372	1950	29	.7845	.0028	-20	130	Charcoal
SA1	200	UBA-29031	2403	32	.7415	.0029	-730	-400	Charcoal
SA1	300	UBA-29032	3194	32	.6719	.0026	-1590	-1400	Charcoal
SA1	410	UBA-29033	5038	44	.5341	.0029	-3950	-3710	Charcoal
SA1	520	UBA-29034	4000	29	.6078	.0022	-2570	-2470	Charcoal
SA1	520	UBA-29035	3746	36	.6273	.0028	-2280	-2030	Plant macro
SA1	630	UBA-29036	5775	32	.4873	.0020	-4710	-4540	Charcoal
SA1	630	UBA-29037	4989	72	.5374	.0048	-3940	-3650	Plant macro

Table 2.3 *(cont.).*

Core	D (cm)	Lab. ID	^{14}C date	±	F^{14}C	±	Calendar range (95%) BC/AD		Material
SA1	670	UBA-29038	5862	48	.4820	.0029	-4840	-4600	Charcoal
SA1	770	UBA-27666	4584	41	.5652	.0029	-3500	-3100	Plant macro
SA2	100	UBA-29039	2243	31	.7563	.0029	-390	-200	Plant macro
SA2	400	UBA-29040	3611	39	.6379	.0031	-2120	-1880	Plant macro
SA2	600	UBA-27665	4693	35	.5575	.0024	-3630	-3370	Plant macro
SA2	600	UBA-29045	2344	79	.7469	.0073	-750	-200	Plant macro
SA2	605	UBA-29046	2920	44	.6952	.0038	-1260	-1000	Plant macro
SA2	640	UBA-29047	3241	33	.6680	.0027	-1610	-1440	Plant macro
SA3	150	UBA-29965	1068	33	.8755	.0036	900	1020	Charcoal
SA3	150	UBA-29966	995	26	.8835	.0029	990	1150	Charcoal
SA3	250	UBA-29967	2536	66	.7293	.0060	-810	-430	Charcoal
SA3	350	UBA-29968	3182	61	.6730	.0051	-1610	-1290	Plant macro
SA3	350	UBA-29969	2910	34	.6961	.0030	-1210	-980	Charcoal
SA3	450	UBA-29970	3765	37	.6258	.0029	-2290	-2040	Plant macro
SA3	450	UBA-29971	1678	28	.8115	.0028	260	420	Charcoal
SA3	550	UBA-29972	3768	43	.6256	.0033	-2330	-2030	Plant macro
SA3	650	UBA-29973			1.0026	.0033			Plant macro
SA3	650	UBA-29974	4978	35	.5381	.0023	-3920	-3660	Charcoal
SA3	850	UBA-29975	5657	37	.4945	.0023	-4580	-4370	Plant macro
SA3	850	UBA-29976	9535	61	.3051	.0023	-9170	-8710	Charcoal
SA3	999	UBA-29977	6125	37	.4665	.0021	-5210	-4960	Plant macro
SA3	999	UBA-29978	6131	35	.4662	.0020	-5210	-4960	Charcoal
SA4	102	UBA-30082	864	35	.8980	.0039	1050	1260	Charcoal
SA4	302	UBA-30083	2953	30	.6924	.0026	-1260	-1050	Charcoal
SA4	302	UBA-30084	3469	32	.6493	.0026	-1880	-1690	Plant macro
SA4	402	UBA-30085	3746	37	.6273	.0028	-2280	-2030	Charcoal
SA4	402	UBA-30086	3559	116	.6421	.0092	-2270	-1610	Plant macro
SA4	1002	UBA-30087	6136	43	.4659	.0025	-5210	-4950	Charcoal
SA4	1002	UBA-30088	5709	36	.4913	.0022	-4680	-4460	Plant macro
SA4	1058	UBA-30089	6240	48	.4599	.0027	-5310	-5060	Charcoal
SA4	1058	UBA-30090	6644	39	.4373	.0021	-5630	-5500	Plant macro
SDC	1140	UBA-34970	3793	39	.6236	.0030	-2400	-2050	Charcoal
SDC	1180	UBA-35578	6262	38	.4586	.0021	-5320	-5080	Charcoal
SDC	1210	UBA-34971	6267	48	.4584	.0028	-5340	-5070	Charcoal
SDC	1320						-2850	-2350	Tarxien-period pot sherd
SDC	1360	UBA-35579	8928	47	.3291	.0019	-8250	-7960	Charcoal
SDC	1474	UBA-35580	5378	35	.5120	.0022	-4330	-4070	Charcoal
SDC	1675	UBA-33282	6260	38	.4587	.0022	-5320	-5070	Charcoal
SDC	1785	UBA-35581	6570	35	.4414	.0019	-5610	-5480	Charcoal
SDC	1826	UBA-35583	6515	35	.4444	.0019	-5540	-5380	Charcoal
SDC	1940	UBA-35582	6451	38	.4479	.0021	-5480	-5340	Charcoal
SDC	2068	UBA-35585	6346	43	.4539	.0024	-5460	-5220	Charcoal
SDC	2285	UBA-35586	7145	39	.4109	.0020	-6067	-5821	Charcoal
SDC	2435	UBA-35587	7977	51	.3704	.0023	-7050	-6700	Charcoal

Table 2.3 *(cont.).*

Core	D (cm)	Lab. ID	^{14}C date	±	F^{14}C	±	Calendar range (95%) BC/AD		Material
SDC	2450	UBA-34972	8030	41	.3680	.0019	-7070	-6770	Charcoal
SDC	2500	UBA-34973	7923	39	.3730	.0018	-7030	-6660	Charcoal
SDC	2539	UBA-34974	7019	40	.4174	.0021	-5990	-5810	Charcoal
SDC	2641	UBA-34975	6894	36	.4239	.0019	-5870	-5710	Charcoal
SDC	2670	UBA-35588	7752	52	.3810	.0024	-6660	-6470	Charcoal
SDC	2910	UBA-31707	8957	44	.3279	.0018	-8280	-7970	Charcoal
WZ1	215	UBA-29042	2707	34	.7139	.0030	-910	-800	Charcoal
WZ1	444	UBA-34967	4316	36	.5843	.0026	-3020	-2880	Charcoal
WZ1	450	UBA-29044	7642	61	.3862	.0029	-6600	-6400	Charcoal
WZ1	458	UBA-27667	0	1	1.0141	.0034			Plant macro
WZ1	458	UBA-28262	4707	31	.5566	.0021	-3630	-3370	Plant macro
WZ2	295	UBA-29043	3428	41	.6526	.0033	-1880	-1630	Charcoal
WZ2	495	UBA-28263	4428	43	.5763	.0031	-3330	-2920	Plant macro
WZ2	521.1	UBA-34969	4366	49	.5807	.0036	-3260	-2890	Charcoal
XEM1	147						1190	1270	Monte Pilato tephra horizon
XEM1	157						786	766	Monte Pilato tephra horizon
XEM1	460	UBA-28265	3704	29	.6306	.0023	-2200	-1980	Plant macro
XEM1	501	UBA-31701	4215	29	.5917	.0022	-2900	-2700	Soil humic fraction
XEM1	565	UBA-25211	3063	49	.6830	.0042	-1430	-1130	Plant macro (Poaceae frags)
XEM1	565	UBA-29048	4571	135	.5661	.0094	-3630	-2930	Charcoal
XEM1	656	UBA-31705	5179	37	.5248	.0024	-4050	-3820	Soil humic fraction
XEM1	670	UBA-29041	5357	39	.5133	.0025	-4330	-4050	Charcoal
XEM1	816.5	UBA-31702	7055	41	.4155	.0021	-6010	-5840	Soil humic fraction
XEM1	864.5	UBA-31703	7273	35	.4044	.0018	-6220	-6060	Soil humic fraction
XEM1	886	UBA-31706	7042	41	.4162	.0021	-6000	-5840	Soil humic fraction
XEM1	923	UBA-31704	7045	44	.4160	.0022	-6010	-5840	Soil humic fraction
XEM1	1000	UBA-25001	9353	58	.3122	.0022	-8780	-8460	Charcoal
XEM2	318	UBA-31708	3124	33	.6778	.0028	-1490	-1280	Charcoal
XEM2	413	UBA-31709	4150	51	.5966	.0038	-2880	-2580	Charcoal
XEM2	508	UBA-29349	4873	33	.5452	.0022	-3710	-3540	Charcoal
XEM2	718	UBA-29350	7399	50	.3981	.0025	-6400	-6100	Charcoal
XEM2	823	UBA-29348	7463	39	.3950	.0019	-6420	-6240	Charcoal
XEM2	933	UBA-29347	8334	46	.3543	.0020	-7520	-7200	Charcoal

is insufficient sediment supply to keep pace with the rate of sea level rise. It was thus possible to infer from the geomorphology of the sites and the pattern of discontinuities that careful choice of borehole locations would enable the assembly of a complete stratigraphic sequence from several boreholes, even if there were discontinuities in individual cored sequences. It was decided to establish basin geometries and identify depo-centres using ground penetrating radar and available borehole records, then sample several locations in each of the coastal plains where deep stratigraphies had been located. This strategy was designed to provide the best possible chance of sampling continuously deposited sediments, with multiple cores to cover hiatuses in individual core sites.

Several borehole sites covering as much as possible of the Maltese Archipelago were necessary if regional patterns of land-use were to be identified. In practice, the number of boreholes was limited by logistical and cost implications, and some of those drilled, such as at Marsalforn, transpired to be in very coarse gravelly sediments unsuitable for analysis.

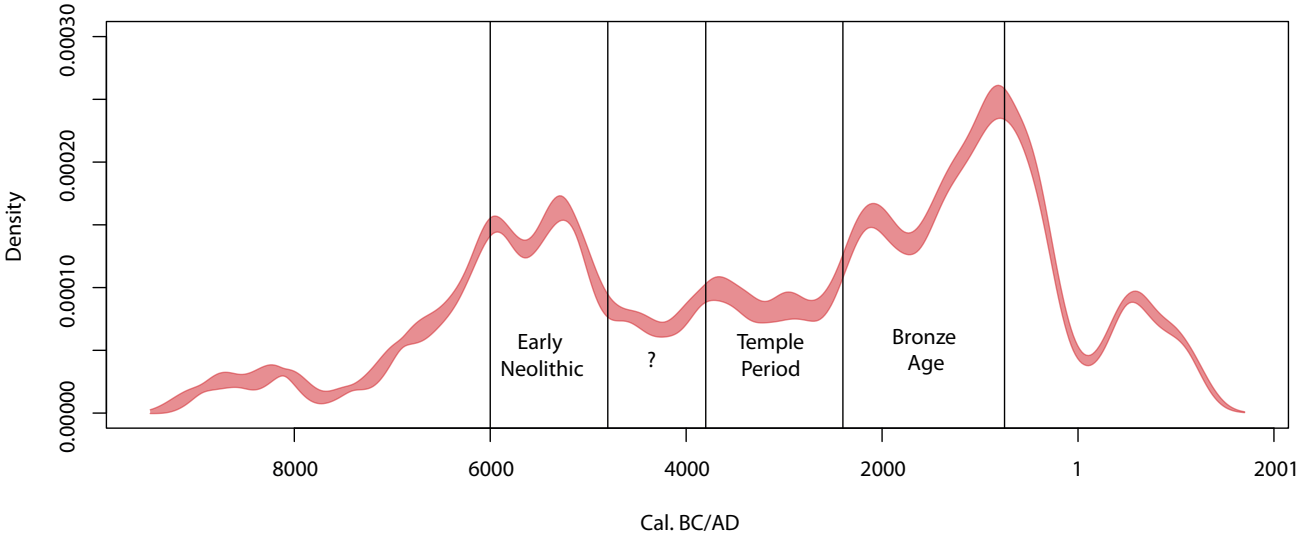

Figure 2.5. *Radiocarbon activity in sediment cores (R. McLaughlin).*

Nevertheless, coverage of the Maltese landscape was more than doubled by the work of the *FRAGSUS Project*. The archaeological sites excavated by the project also contributed samples for palynology, anthracology, plant macro-remains and soil micromorphology.

A particular challenge faced by the *FRAGSUS Project* was the need to reach sediments earlier than those that had been sampled by previous studies, and thereby establish the environments and vegetation present before human colonization of the Maltese Islands. This required extremely deep boreholes, because coastal sedimentation was, and is, controlled by sea level. From a low of about -120 m at *c*. 18,000 BC, sea level rose extremely rapidly in the central Mediterranean. Lambeck *et al*. (2011) suggested sea levels of about -60 m at 10,000 BC, -45 m at 8000 BC, -30 m at 7250 BC, -20 m at 6500 BC and -10 m at 5500 BC, although this might be mitigated locally by crustal levering caused by loading of continental shelves during sea level rise. This suggests that sea level controlled sedimentation might be at or below these depths during the Holocene, and consequently that a slight increment in time would necessitate a considerable increase in the depth of sampling needed. In practice, issues of opportunity, logistics and expense limited the number of very deep boreholes to one, at the Salina salt pans, where geotechnic boreholes indicated that a very deep valley fill was present.

Prospective coring locations were identified from the literature, from maps and aerial photographs, the ground penetrating radar surveys (GPR; see §2.2 above) (Fig. 2.3), and by consultation and discussion with *FRAGSUS Project* team members. Permissions were obtained by the officers of Heritage Malta and the Superintendence of Cultural Heritage, Malta. As there was limited time to drill multiple boreholes, geophysical survey using ground penetrating radar with a 10 m aerial was used to establish the deepest and most complete stratigraphy and thus optimal coring locations. At most prospective localities, the geophysical trace identified the rock-head profile, but at Salina and some coastal locations in south Malta the trace was lost as the result of salt-water intrusion and/or a predominantly clay fill. Core locations were surveyed using differential GPS (dGPS) with full descriptions and granulometry of the cores extracted by the *FRAGSUS Project* in Appendices 3 and 4, with the radiocarbon dating results listed in Table 2.3 (Figs. 2.1, 2.2 & 2.5).

Open-chambered percussion piston augers made by Eijkelkamp were used in very stony deposits. Where possible, paired boreholes were drilled with Eijkelkamp percussion piston order, with cores one metre in length and 5 cm in diameter recovered in rigid plastic liners. A core-catcher was often necessary as the sediments were largely unconsolidated. Core recovery was generally good but hydro-collapse occurred in several core segments in boreholes penetrating the shell gravels at Salina. Cores were stored in the Queen's University Belfast cold store at 4°C prior to splitting and analysis.

The Salina Deep Core was recovered by SolidBase Lts using a shell and auger rig and 8 cm diameter percussion cores 0.5 m in length in groups of three. At this site, the top part of the sequence was in shell gravel which hydro-collapsed and fell from the samplers. Recovery started at *c*. 11 m where silt- and clay-based

sediments began. The recovered sediment sequence was stored in a refrigeration unit at 4°C in Liverpool John Moores University prior to extrusion and analysis.

2.3.2. The core descriptions

2.3.2.1. The Salina Deep Core

The Salina Deep Core was drilled at the edge of an extensive complex of salt pans built by the Knights of St John towards the end of the sixteenth century on marshland at the entrance to the large Burmarrad plain. A fine plan of the complex executed in AD 1742 by the Order's surveyors show the pans as they were extended in AD 1650, with large reservoirs meant to hold seawater before it was channeled into the salt pans (Blouet 1963; National Library of Malta, Treas. B290, f. 23a). The complex was the property of the Grand Master who controlled the use of salt as a condiment and for curing meats (Mercieca 2005). The Burmarrad plain was considered to be good quality land in the first survey carried out by the Order in 1654, given over to the growing of grain, cotton and cumin (Blouet 1963). In 1658, halophytic vegetation that grew at the seaward end is known to have been collected and burnt, with the ash sold as a fertilizer (Blouet 1964). The salt pans are located in an area that was documented as an anchorage in the late fifteenth century and a watch tower stood on the shore at least a century earlier (Dalli 2011). The remains of rock-cut burial complexes of Late Roman date along the east shore, other remains discovered during construction works over the last twenty years, and a large Roman farming estate located on higher ground at San Pawl Milqi to the southwest suggest that the area saw major maritime-oriented activity in Roman times (Marriner *et al*. 2012). This may also be said of an earlier period, when the bay appears to have extended further inland. A Neolithic temple stood on the rocky, eastern edge of the plain at Tal-Qadi while a tomb was cut in the rock in the Żebbuġ phase where the Roman estate was subsequently built (Evans 1971; Cagiano de Azevedo 1969; Grima 2011a).

At Salina, the geotechnical boreholes drilled in preparation for the rehabilitation of the salt pans showed a deep valley fill, as recorded here and in the Burmarrad valley by Carroll *et al*. (2012) and Marriner *et al*. (2012). The Salina valley is highly asymmetric, but close to the northeastern margin of the pans is over *c*. 30 m deep. However the base of the valley fill was not reached. Here, the top part of the Deep Core borehole passed through shell gravel which hydro-collapsed and fell from the samplers, but the same unit was encountered in a nearby borehole (Salina 2 core, see Appendix 2) drilled with a percussion auger by the *FRAGSUS Project*. Recovery of the deep core started at *c*. 11 m where the sequence passed into silt- and clay-based sediments.

The sediments encountered in the Salina Deep Core are shown in Tables 2.4 and A3.1. The borehole was drilled through the trackway at the edge of the salt pans. After passing through *c*. 2.4 m of rubble and masonry, the borehole then passed through *c*. 8.6 m of shallow marine shell gravel, then *c*. 2 m of shallow marine sandy shoal sediments, *c*. 8.0 m of distal pro-deltaic muds, 5.65 m of delta-front and pro-deltaic sediments interbedded with lower energy quiet water sandy muds, 0.35 m of littoral marine muddy gravels, 2.3 m of fluvial gravels, and a *c*. 0.17 m thick silty clay palaeosol, all developed on Globigerina Limestone. AMS radiocarbon dates range from 8280–7970 cal. BC (8957 BP; UBA-31707) at 29.1 m to 4330–4070 cal. BC (5378 BP; UBA-35580) at 14.74 m to 2400–2050 cal. BC (3793 BP; UBA-34970) at 11.4 m below the ground surface (Table 2.3), with an age-depth model suggesting a start to sediment accumulation from at least 7500 cal. BC (Table 2.5).

This sequence can be interpreted as reflecting the development of a terrestrial valley fill and then the drowning of the valley by rising sea levels. The initial valley fill is composed of pedogenically altered muddy hillslope deposits (colluvium) and gravelly alluvium of a multi-channel ephemeral river. It formed during the Late Pleistocene/early Holocene phase of low sea level. The hillslope deposits are consistent with a lightly vegetated and most probably seasonal semi-arid landscape, as are the very poorly sorted fluvial gravels. The carbonate forms and soil development in general are also consistent with strong seasonal aridity.

Littoral gravels record the flooding of the valley by rapidly rising sea level during the Early Holocene. The delta-front and pro-delta deposits overlying these suggest initially deepening water as sea level continued to rise. Very quickly, however, the drowned valley started to infill with the products of soil erosion from the Burmarrad catchment. Soil eroded during high rainfall events was carried seaward by the Burmarrad River and a delta must have developed and then migrated up-valley as sea level rose. Off the delta front, the river water, dense with suspended sediment, will have spread across the sea floor as a series of gravity-driven turbidity currents. The waters in the Salina inlet therefore probably never became very deep, as sedimentation was extremely rapid, but the finely layered sediments comprising most of the pro-deltaic sediments will most probably have been laid down in waters deeper than wave-base. During periods between major floods, the sea bed would have been colonized by marine animals, and bioturbation

will have occurred, leading to massive (structureless) sediments, whereas the turbidity flows will have repeatedly killed benthic animals, thus leading to well laminated sediments undisturbed by burrowing organisms. As sea level rise slowed from *c*. 3000 BC onwards, the sedimentation rate will have exceeded the rate of sea level rise and the waters in the Salina inlet will have shallowed, with the sea coming within wave-base, allowing winnowing to occur during storms. The winnowing will have re-suspended silt and clay, which will have been transported seaward, leaving behind the shelly shoal sands. As the waters of the inlet continued to become shallower, winnowing will have intensified and sand-sized material will have been carried seaward. The shell gravels at the top of the sequence developed in shallow, turbulent waters, with accommodation space and thus sedimentation rate being constrained by the declining rate of sea level rise in the later Holocene. During this time, fine sediments resulting from soil erosion in the Burmarrad catchment will have been carried past the shell-gravel shoals into deeper water.

2.3.2.2. The Salina 4 core

The nearby Salina 4 core was some 11.02 m in depth (Tables 2.4 & A3.2). AMS dates range from 5630–5500 cal. BC (6644 BP; UBA-30090) at 10 m to 1260–1050 cal. BC (2953 BP; UBA-30083) at 3 m and cal. AD 1050–1260 (864 BP; UBA-30082) at 1 m depth (Table 2.3). The basal *c*. 3.5 m is dominated by estuarine sediments of fine sandy silty muds below a *c*. 3 m thick zone of alternating silty clay and fine sandy muds. These sediments are pro-deltaic in origin. The overlying zone between 4.38 and *c*. 3 m depth consists of alternating grey and black silty clays and was slightly shelly sand which hydro-collapsed during extraction. Above this was a metre of olive grey silty clay lagoonal sediments. The upper *c*. 2 m of the core was dominated by yellowish orange and brown silt clays with silty sand lenses between *c*. 0.82–0.58 m down-profile. These appear to be overbank flood deposits accumulating in a back-basin lagoon. This stratigraphy suggests an original estuarine depositional setting close to the mouth of the Burmarrad River. Deposition outpaced sea level rise so the sand unit was deposited, probably rather rapidly, within the wave-base, before the progradation of fluvial overbank deposition across the site. The silt/sand alternation in the top two metres of the core is consistent with vigorous flooding from the Burmarrad River.

2.3.2.3. The Salina 2 core

The core was drilled through the base of the drained Salina saltpans to a depth of 7.9 m before drilling was abandoned in what was probably hydrocollapsing shell gravel, but core recovery, even with the core catcher, started only at 6.54 m. The basal ~5.3 m of the recovered core consists of alternating grey and dark grey-brown very shelly coarse sands/sandy gravels and highly organic sandy silty clays. Some of the sandy silty clays had eroded or burrowed tops, consistent with pauses in deposition of unknown duration and some of the coarser sandy shell-gravel units hydrocollapsed on extraction. These units probably reflect shallow offshore deposition in sandy gravel shoals bearing eel-grass meadows and sheltered, quieter-water inter-shoal environments, respectively, suggesting that the floor of the outer estuary was covered with shifting sandbars. Above 1.27 m in the core, littoral sands alternate with shallow estuarine sediments, suggesting that this part of the estuary had shallowed sufficiently that the sandbars were sometimes emergent.

2.3.2.4. The Xemxija cores

Two cores were taken in a modern pine grove located immediately behind the road that skirts the sandy beach at Pwales, a summer resort that extended along the Pwales Road in the post-World War II period. Documentation shows that the area where the cores were taken formed part of an estate consisting of seven hectares of marshland located behind the foreshore. These were drained in AD 1650 and had been transformed into good quality arable land surrounded by walls and equipped with drainage channels by AD 1658 (Blouet 1964). A plan drawn by the Order's surveyors in AD 1784 shows the extent of the estate (National Library of Malta, Treas. B301, f. 57). The channels can be clearly made out in the western fields as rectilinear anomalies in aerial photographs; some were destroyed when the area was turned into a nature reserve in the early 1990s, as was a large farmhouse that stood in the middle of the estate. The whole area is prone to severe flooding and this happened at least twice in the last century, in 1957 and 1982 (Bowen Jones *et al*. 1961). A small chapel was built further into the valley in AD 1672, where several springs created water gardens. Archaeological remains of note are concentrated not on the plain but higher up on the ridge to the north and consist of a series of Neolithic shaft-and-chamber tombs cut into the rock (Evans 1971), and the remains of an unexplored Neolithic temple at Ta' Żminka (Vella 2002) located on the eastern edge of an olive grove that was planted as part of an afforestation project carried out in 1957. A rock-cut tomb nearby dating to the third century BC (Vella *et al*. 2001), and other caves with evidence of contemporary and later use located along the escarpment overlooking Mistra Bay,

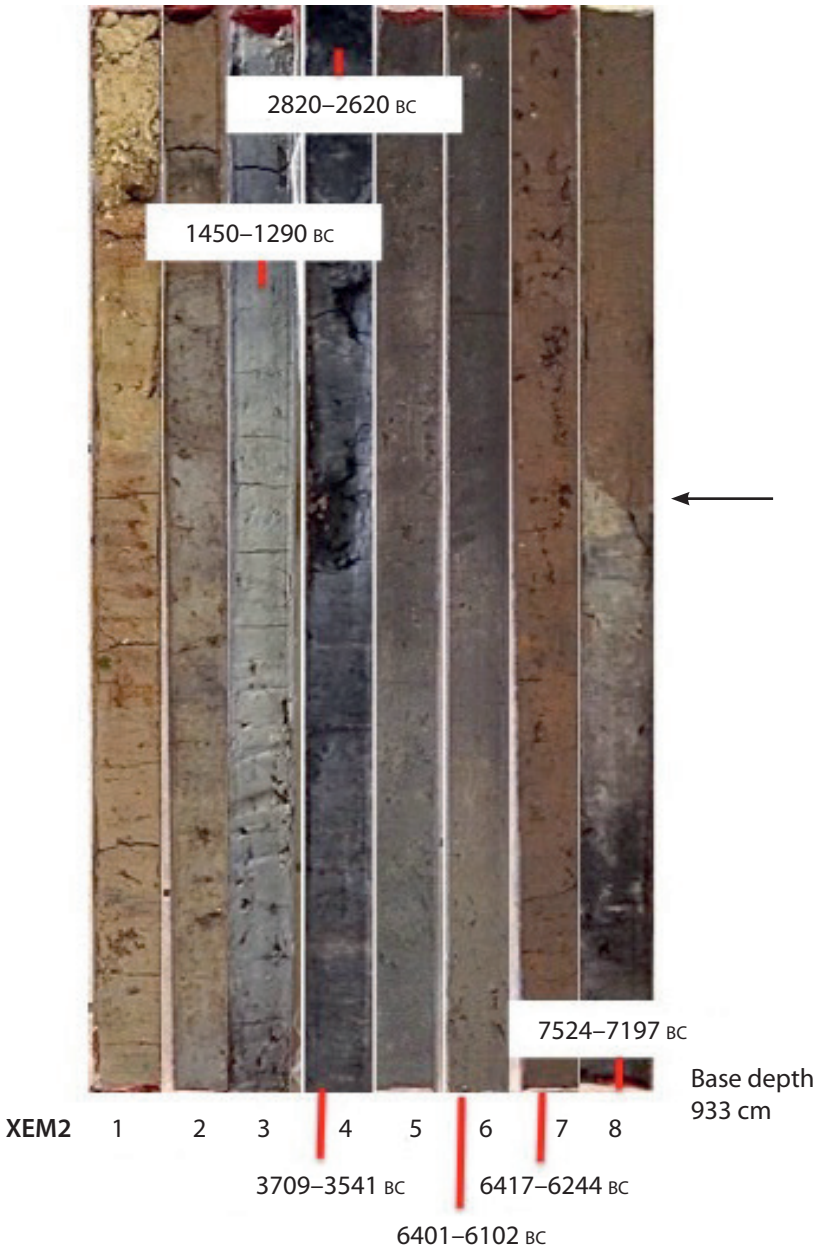

Figure 2.6. *The Xemxija 2 core by depth with the arrow indicating the cumulative palaeosol/mass-flow transition (K. Fenech).*

show that a small community was established here in Late Punic times, possibly exploiting the agricultural potential of an area that saw several attempts at agricultural improvement throughout the Knights and British periods (Hunt & Vella 2004/5).

Two *c*. 10 m deep cores (XEM 1 & 2) were taken, about 2 m apart, with overlapping core segments. They have broadly similar stratigraphy and chronology (Tables 2.4, A3.4 & A3.5). In the basal metre of the 10 m Xemxija 1 core, there is a silty clay loam cumulative soil with some structure and an organic component which began to accumulate from at least 8780–8460 cal. BC (9353 BP; UBA-25001), with sedimentation continuing to more or less the present day (Table 2.3). This basal cumulative soil is very calcitic, indicative of calcareous groundwater and strong seasonal drying, and was most probably an aggrading alluvial soil. Above this, there is a further *c*. 3.4 m of similar mass-flow silty clay material that accumulated in marshy conditions which contains occasional to frequent limestone fragments and pebbles. These deposits may be indicative of greater erosion and exposed limestone substrates in the immediate catchment. Interrupting this aggradation are three layers with finer sediments, weak pedogenic structures and some organic accumulation, suggestive of a slowing of aggradation and

incipient organic A horizon formation at several points up-profile (at 8.15–8.32, 6.7–6.85 and 6.0–6.3 m). These essentially indicate periods of some stabilization of the floodplain surface (see Chapter 5).

There is then a major change in the system with the accumulation of a thick layer of black organic silt mud between *c.* 5.65 and 4.6 m, after about 4330–4050 cal. BC (5357 BP; UBA-29041) and up to at least 2200–1980 cal. BC (3704 BP; UBA-28265) (Tables 2.3 & 2.4). This suggests that there was a lengthy phase of near permanent, shallow standing water, and only minimal input of very fine eroded soil material in this shallow freshwater 'lagoonal' or paludal (marshy) situation, probably behind a bay-bar.

Subsequently, there was a return to fine alluvial calcareous silt accumulation, interrupted by the occasional coarser layer (at 2.5–2.65 m) or incipient palaeosol (at 3.19–3.35 m), (see Chapter 5; Fig. 2.6; Table 2.4; Appendix 3).

2.3.2.5. The Wied Żembaq cores

The low, steep-sided spur or ridge known as Borġ in-Nadur, overlooking the small cove of St. George's Bay in southeast Malta, is defined by two converging deep valleys, the Wied Żembaq to the west and the Wied Dalam to the east. The area has witnessed a long history of human occupation, including a Neolithic temple that was re-used during the Bronze Age when a settlement flourished behind an impressive fortification wall that cut right across the spur and appears to have followed the entire perimeter of the ridge (Tanasi & Vella 2011a & b, 2015). Remains of two dolmens are

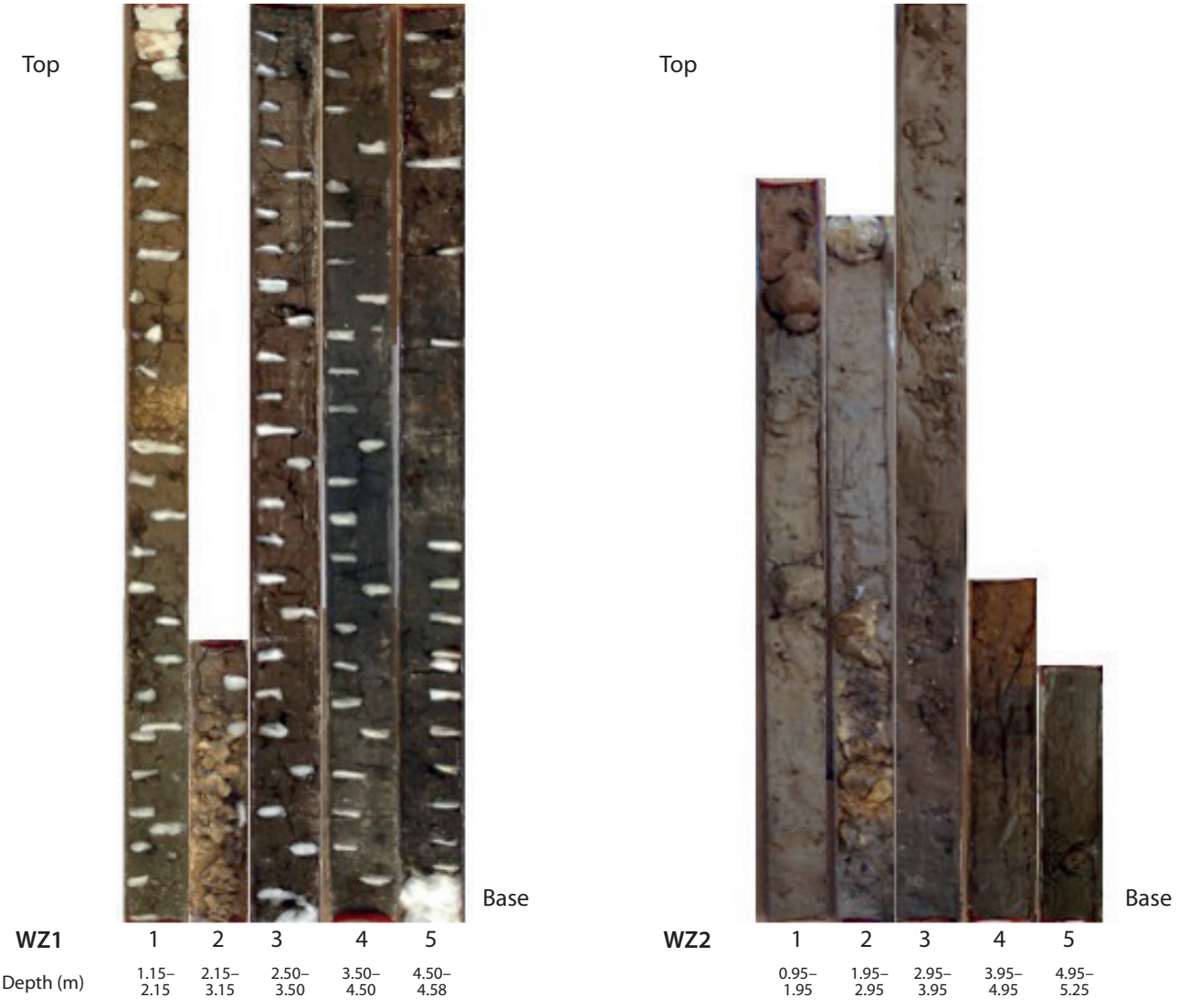

Figure 2.7. *The Wied Żembaq cores 1 (left) and 2 (right) by depth (K. Fenech).*

also known, one near Borġ in-Nadur and the other on the high ground to the west of Wied Żembaq (Evans 1971). On the southern side of the Wied Dalam, on sloping ground at Ta' Kaċċatura, a large Roman villa site with a peristyled courtyard was excavated at the turn of the last century. This contained equipment that was used for extracting olive oil (Anastasi & Vella 2018). A rock-cut burial found on higher ground would appear to be contemporary. Historic records from the mid-seventeenth century identify St George's Bay with marshland, used for retting flax and drained in AD 1736 (Abela 1647; Blouet 1964). Quarrying can be noted along the edges of both valleys where the alluvial plains have been transformed into fields divided by low-lying rubble walls. Some documentary evidence from AD 1750 shows that the valley bottom, right below the Roman villa and extending towards the sea, was planted with trees (National Library of Malta, Treas. B303, f. 128). The fields at Wied Żembaq were probably exploited in a similar manner in the historic period, and they were certainly being worked when the core was taken.

Two cores were taken from the Wied Żembaq (Fig. 2.7; Tables 2.4, A3.6 & A3.7). Core 1 has a basal *c*. 1.8 m of organic silty mud with occasional large limestone blocks, interspersed with layers of less organic silty loam at 4.5–4.8 m and 4.2–4.5 m. The upper part of the core is composed of *c*. 3.64 m of silt loam alluvial material with three layers of sub-angular silty gravel. There are AMS dates of 3630–3370 cal. BC (4707 BP; UBA-28262) at 4.58 m and 910–800 cal. BC (2707 BP; UBA-29042) at 2.15 m (Table 2.3). The core is interpreted as a progression from a basal dark grey to black clay accumulating in shallow standing water from 4.84–5.48 m to stony overbank alluvial sedimentation at 4.51–4.84 m, with occasional inputs of coarse sediment and hillwash from the steep side of the valley, to a shallow water marsh at 3.71–4.51 m, with renewed alluvial activity above.

The Wied Żembaq 2 core profile had significant breaks caused by the loss of material from the core. The basal unit (5.13–4.2 m) consists of an organic silty mud salt marsh deposit with occasional large limestone blocks. This passes up into silt loams with occasional stony layers, then further organic silty mud (4.2–3.85 m), then a shallow, saline lagoon deposit at 3.85–2.96 m. Traces of pedogenesis including blocky peds and strong reddening are visible at 5.28, 4.33, 3.65 and 3.0 m (Table A3.7). There are AMS dates of 3330–2920 cal. BC (4428 BP; UBA-28263) at 4.95 m and 1880–1630 cal. BC at 2.95 m (3428 BP; UBA-29043) (Tables 2.3 & 2.4). Above 2.96 m the core contains brown sandy clay colluvium to 1.15 m below ground surface.

2.3.2.6. The Mġarr ix-Xini core

This core was drilled in the narrow alluvial plain behind the pebbly beach at Mġarr ix-Xini on the southern coast of Gozo. The beach is located at the end of the meandering, deep-sided Wied Ħanżira gorge. Relict phreatic features and cave sediments on the gorge wall suggest that this feature originated as a collapsed cave. A photograph from the early 1930s shows cultivated fields in the area coming right up to the shore, with sufficient space for a watercourse running along the southern edge. A number of hydrological features, including a building housing a water pump built in the 1890s, an aqueduct and a series of dams can be found along the gorge – all attempts to control and harvest water run-off. Early last century, on the Ta' Ċenċ and Sannat uplands to the west, archaeologists discovered several prehistoric sites including the remains of a Neolithic temple at Borġ l-Mramma and at least two dolmens, one at Ix-Xagħra il-Kbira and another at Id-Dura tal-Mara, besides numerous cart-ruts (Evans 1971; Magro Conti & Saliba 2007). Neolithic temple remains were also recorded on the Xewkija side of the valley, where the present parish church stands (Evans 1971; Magri 2009 (1906)). The Mġarr ix-Xini cove was known to have provided a safe haven for small boats throughout history, and a tower was built by the Order of St John at the eastern tip in 1661 to watch over maritime traffic along this stretch of sea. Recent archaeological investigations within the gorge have attempted to understand the function of 17 rock-cut threading pans and vats that are found on the exposed rock surface of the tightly curved meanders and along the bottom of the escarpment. It is thought that some of the features may date to Late Punic or Roman times and would have served to make wine (Pace & Azzopardi 2008; Bonanno 2008) (see Chapter 7). Two hard limestone mills discovered at Tas-Salvatur and Tal-Ħamrija indicated that olive oil was also produced in the vicinity during Roman times (Anastasi & Vella 2018). The remains of a rural shrine from the same period have been found in a restructured cave site at Għar ix-Xiħ, overlooking the cove (Azzopardi 2014).

The basal *c*. 3.9 m of the 7.43 m deep Mġarr ix-Xini core is dominated by fining-upward sequences of poorly sorted gravels, coarse sand and sandy muds, with a silt horizon at 5.84–5.72 m and fine sandy silty clays between 6.17–5.82 m (Fig. 2.8; Tables 2.4 & A3.8). AMS dates range from 1490–1290 cal. BC (3124 BP; UBA-29989) at 7.17 m to cal. AD 690–880 (1230 BP; UBA-29980) at 1.76 m depth (Tables 2.3 & 2.4). The sequence above becomes marked by a calcitic sandy mud, which may be an incipient palaeosol at 3.55–3.3 m, then gravelly sands at 3.09 m overlain by a lens of massive pure clay to 3.06 m. Above was 2.98 m

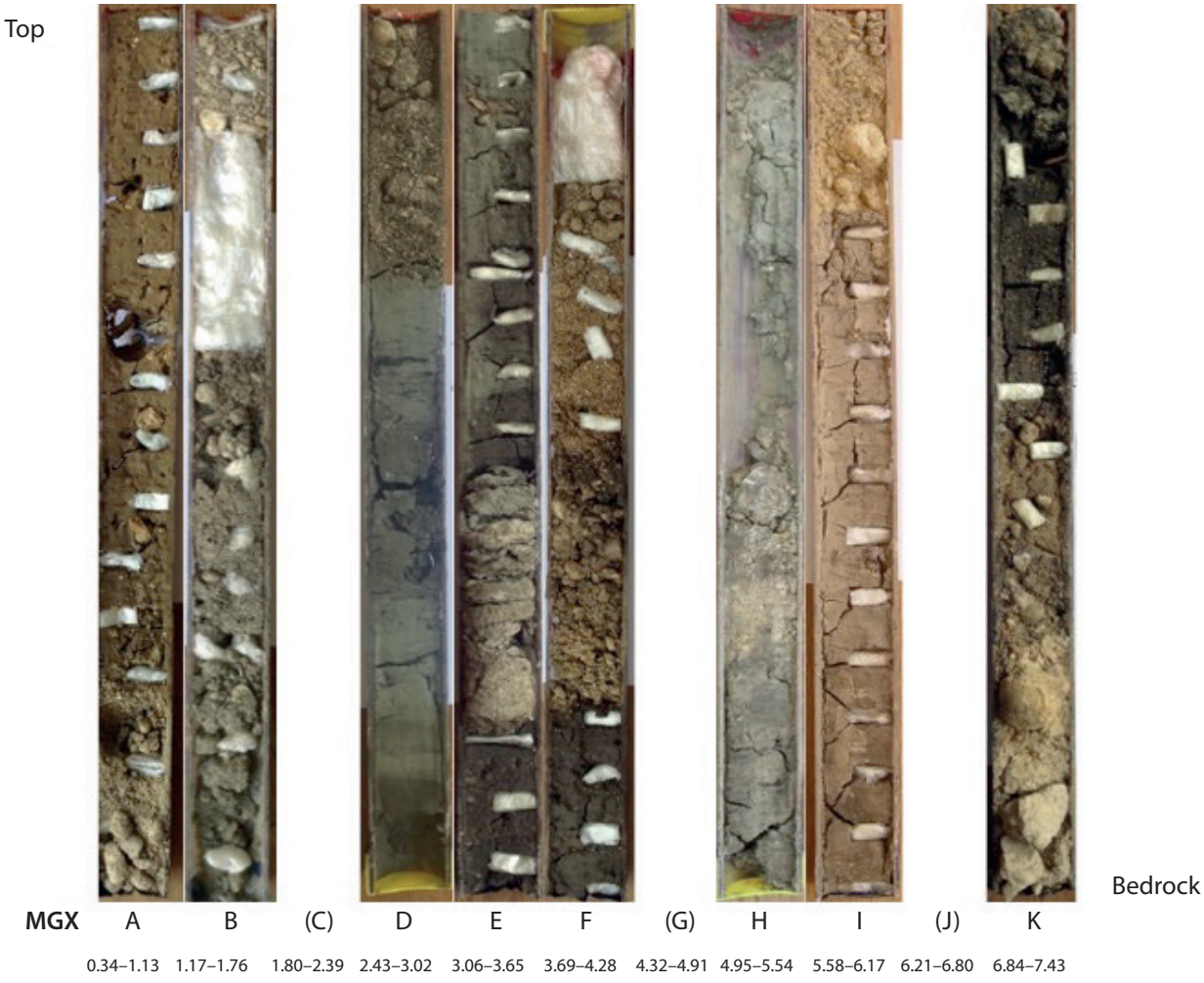

Figure 2.8. *The Mġarr ix-Xini core by depth (K. Fenech).*

of a finer unit of clayey silts interspersed with grey fine sandy silt and coarse clastic shelly sands indicative of a shallow marine environment. This shallow marine setting experienced occasional energetic storm run-off that introduced coarse sediment, which would have been carried across the sea bed to the core site by turbidity currents. Shifting of the river-mouth and the sub-marine thalweg of the turbidity currents will have controlled the coarseness of the sediments. As the coast prograded it is likely that the turbidity currents carried the coarse clastic sediments past the core site and further out to sea, so the site became dominated by shallow marine sedimentation. Coastal progradation was slow, only advancing across the core site within the last thousand years.

2.3.2.7. The Marsaxlokk 1 core

Two cores were attempted and one core was taken from an area adjacent to a salt marshland known as Il-Ballut ta' Marsaxlokk, a designated nature reserve, located on the edge of the fishing village. Fishponds, of unknown antiquity, existed here until they were dredged to make way for a quay in the 1950s. It is hypothesized that the small inner harbour, known as Il-Magħluq, could have existed in some shape or form in antiquity possibly providing shelter for the seacraft that would have used this area in connection with activities that took place at the site of Tas-Silġ, less than a kilometre away up the hill in the direction of Żejtun (Bonanno 2011). Tas-Silġ flourished in Late Neolithic times as a sanctuary that was adapted, transformed and extended in successive historic periods as an extra-urban maritime sanctuary in Punic and Roman times and subsequently as a church with a baptismal font (Cazzella & Recchia 2012; Bonanno & Vella 2015).

The base of core 1 has *c.* 1 m of reddish brown calcitic, stony, silty clay loam (3.46–2.92 m) with a well-developed small, sub-angular blocky structure,

and its groundmass is dominated by a slightly calcitic, silty clay with moderate to strong amorphous sesquioxide reddening (Fig. 2.9; Tables 2.4 & A3.9). This unit is probably a *terra rossa*-type palaeosol. Its upper surface is truncated and overlain by a layer of fine beach gravel and coarse sand deposits and then *c*. 2.86 m of calcitic fine sandy/silt loam. This deposit was receiving terrestrial clastic material in the form of coarse sand/fine gravel, with lenses at 1.92–1.86 m and 1.65–1.55 m, and an organic silt mud layer of likely paludal origin at 1.7–1.65 m. This layer is probably overbank alluvium, or more likely, given the location, hillwash. Two AMS radiocarbon dates more or less overlap in the first half of the first millennium AD (1567 BP; UBA-29353; and 1444 BP; UBA-29351) and a third date is 540–380 cal. BC (2354 BP; UBA-29352) (Table 2.3), suggesting that these deposits are mixed and have probably accumulated over a relatively recent and short time.

2.3.2.8. The Marsa 2 core

Marsa is the largest alluvial plain in Malta, characterized by high ground that rises to the north, south and west. Tributary valleys, especially Wied is-Sewda and Wied il-Kbir, drain into the area now occupied by the Marsa Sports Ground, a complex that was used for the recreation of British servicemen since the 1860s and more recently for a variety of sports including horse-racing, athletics and cricket. Two cores were taken near the eastern entrance to the complex before new building works commenced, which were part of a redevelopment of the site in 2002 (Fenech 2007;

Figure 2.9. *The Marsaxlokk cores 1 (left) and part of 2 (right) by depth (K. Fenech).*

Carroll *et al*. 2012). Despite the absence of Neolithic structures in the plain, human activity there could be ascertained through the presence of several pottery sherds found in the scattered sediments, the earliest dating back to the Ġgantija phase, *c*. 3450–3200 BC. Two inlets join the floodplain to the sea at the head of Grand Harbour. The first of these, Marsa iz-Zgħira (or *Marsetta*, present-day Menqa), lies to the north of the promontory called Jesuits Hill, where, in 1768, Roman warehouses were discovered with clear evidence for use well into Medieval times, together with the remains of a quay uncovered in 1993 (Bruno & Cutajar 2002). The second is Marsa il-Kbira (or *Marsa Grande*, present-day Marsa Creek) to the south of Jesuits Hill and northwards of a limestone knoll or islet (*Isolotto*, *il-Gzira*) where Albert Town developed in the late nineteenth century. Archaeological remains have been recorded in the immediate environs, including tombs and remains of warehouses (Gambin 2008; Bonanno 2011). The Marsa plain and immediate environs are known to have been an important source of revenue for state coffers in Late Medieval times (Bresc 1975). Sedimentation in the inlets led to attempts to drain the marshland, certainly by AD 1650, to create new agricultural land with drainage channels excavated to ensure that storm water ended up in the sea, of a sufficient depth to allow small boats to proceed to the plain in the direction of the Late Medieval chapel located at Ta' Ċeppuna (Blouet 1963, 85).

The Marsa 2 core was extracted at a level of 1.18 m above mean sea level and had a total depth of 9.40 m (Tables 2.4 & A3.10). The bedrock was at 9.25 m. Dense coarse strong-brown to reddish yellow sandy muddy gravel extended from 9.25 m to 6.40 m with a large boulder between 7.00–6.75 m. These sediments are interpreted as a delta-top or delta front facies. From 6.40 m, the sediments were no longer oxic but were dark grey and waterlogged. From 6.20 m, gravel and sand increased relative to fines, and between 5.90–5.20 m the sediments were too sandy to be recovered. It is likely that these are proximal pro-deltaic sediments. Datable organic remains were very scarce and the earliest radiocarbon date at 5.98 m was 980–840 cal. BC (2765 BP; UBA-30608), in the Phoenician era (Table 2.3). The sediments between 5.20–3.90 m were alternating silt/clay and sand layers and are dark grey. These are most probably distal pro-delta sediments. From 3.90 to 1.95 m the sediments are pale grey with the silt/clay content increasing, probably because the water body was bypassed by gravity currents at this time. A radiocarbon date at 2.70 m gave a Late Roman period date of cal. AD 430–650 (1487 BP; UBA-29443) (Table 2.3). An event shortly after that time resulted in the deposition of a boulder between 2.55–2.20 m in the core. From 1.95 m upwards, the sand content increases and the sediments are very light grey, most probably deposited in a shallowing water body. Another boulder between 1.70 m and 1.20 m was overlain by light brown silty sediments, which are most probably delta-top overbank deposits. Above 0.95 m, the area appears no longer to have been waterlogged as a result of further overbank deposition. While penetrating the groundwater table, sediments between 0.8 and 0.3 m could not be retained by the corer. The uppermost 0.3 m of the core was predominantly light brown silts of fluvial overbank and slopewash origin, in agreement with the present day terrestrial conditions at the coring site.

2.3.2.9. The Mellieħa Bay core

Marshland at Mellieħa Bay lies behind a bay-bar of what were low dunes at the back of the sandy beach, although the dunes are now mostly covered by the main road. The core was taken by the entrance to the Nature Reserve on the landward side of the present road. The marshland lies to the north of a low limestone ridge which bisects the plain. The marsh was used for the collection of salt in the early sixteenth century (Mercieca 2005). By AD 1658 the marshland had been drained and equipped with channels, and vegetation that could be burnt and used as fertilizer was collected (Blouet 1964). No archaeological remains have been recorded in the immediate vicinity, but Neolithic megalithic remains were recorded on the southern rocky shore of the bay at Għajn Żejtuna (Evans 1971) and an undated burial was discovered a few years ago in the grounds of the Mellieħa Bay Hotel. A photograph of the pottery contents of a Phoenician tomb from the end of the eighth century BC is labelled 'Mellieħa' and would suggest that Levantine seafarers operated in this area at this early date (Vella 2005). A wreck from the first–third centuries AD excavated around the rocks in the middle of the bay in 1967 would suggest that Mellieħa was frequented in Roman times (Frost 1969). The higher karst ground to the west has been known to be used for rough grazing since the seventeenth century and was certainly used for this purpose in the twentieth century. The slopes to the north, below the ridge of Il-Qammieġħ and L-Aħrax, were improved considerably in the course of the seventeenth and eighteenth centuries, certainly in the later nineteenth century, when the area, which is now equipped with terraces and a service road, was given over by the British administration on long-term agricultural leases (Blouet 1963; National Library of Malta, Treas. B303, f.145A).

The undated (date failure) 5.36 m deep core has a basal unit of grey, organic-rich silty sandy clay containing eel grass fibres and occasional shell (Tables 2.4 & A3.11). This is an offshore sediment deposited

Table 2.4. *Summary stratigraphic descriptions of the sequences in the deep core profiles.*

Core and depth (m)	Stratigraphic description	Age
Salina Deep Core:		
0–2.4	Rubble and masonry	
2.4–11	Marine shell gravel	
11–13	Sandy marine shoal	at 11.4 m: 2400–2050 cal. BC
13–21	Distal deltaic muds	at 14.74 m: 4330–4070 cal. BC
21–26.65	Delta-front and proximal pro-deltaic sandy muds, interbedded with quiet water laminated sediments	
26.65–27	Marine sediments, probably sub-littoral or upper delta-front muddy gravels	
27–28.5	Fluvial gravels with pedogenic features	
28.5–29.3	Fluvial gravels	at 29.1 m: 8280–7970 cal. BC
29.3–29.47	Palaeosol of silty clay with occasional rootlets and fine charcoal	
29.47+	Globigerina Limestone bedrock	
Salina 2:		
0-1.27	Alternating littoral sands and shallow estuarine sandy silty clays	
1.27-6.54	Alternating organic silty sandy clays and coarse to very coarse very shelly sands	
Salina 4:		
0–0.58	Missing	
0.58–2	Alternating brown and yellowish orange silty clays: overbank flood deposits	
2–4.1	Alternating grey/black silty clays with slightly shelly sand which hydro-collapsed during extraction	at 3 m: 1260–1050 cal. BC
4.1–11.02	Alternating pro-deltaic sandy muds, sands, silty clay and shelly gravel	at 10 m: 5630–5500 cal. BC
Xemxija 1:		
0–4.53	Greyish brown/grey clayey silts and silty clays: overbank flood deposits, with incipient palaeosol at 3.19–3.35 m	
4.53–5.67	Shallow freshwater lagoonal or paludal marsh deposits of shelly organic silty clays and fibrous peat	at 4.6 m: 2200–1980 cal. BC
5.67–6.03	Mud flow deposits of silty clay and clay aggregates	
6.03–6.38	Dark greyish yellow silty clay with weak soil development	
6.38–6.68	Mud flow deposits of silty clay and clay aggregates	
6.68–9.09	Alluvial deposits of alternating brown/grey silty clays, interrupted by two phases of weak pedogenesis at 6.7–6.85 and 8.15–8.32 m	at 6.7 m: 4330–4050 cal. BC
9.09–9.93	Palaeosol of dark brownish grey very fine sandy silty clay with fine limestone gravel down-profile	
9.93–10	Breccia of silty clay soil aggregates and fine limestone gravel	at 10 m: 8780–8460 cal. BC
Xemxija 2:		
1.17–1.36	Made ground and modern topsoil	
1.36–6.12	Orangey brown over grey alluvial silty clays	at 3.18 m: 1490–1280 cal. BC
6.12–7.17	Organic silty clays: marsh and alluvial deposits	
7.17–8.91	Alternating mixed deposits of greyish brown silty clay, clay aggregates with fine limestone, charcoal, shell and wood fragments	at 7. 18 m: 6400–6100 cal. BC
8.91–8.99	Dark olive brown clay distal mud-flow deposit	
8.99–9.33	Breccia of clay aggregates	at 9.33 m: 7520–7200 cal. BC
Wied Żembaq 1:		
1.16–3.49	Alluvial sandy clays and clays	at 2.15 m: 913–806 cal. BC
3.49–3.64	Yellowish brown silty clay with limestone fragments: probable mud-flow deposit	

Table 2.4 *(cont.).*

Core and depth (m)	Stratigraphic description	Age
3.64–3.71	Brown fine sandy clay with possible incipient soil formation	
3.71–4.51	Dark grey humic clay laid down in marsh/shallow standing water	
4.51–4.84	Stony alluvial clay	at 4.58 m: 3630–3370 cal. BC
4.84–5.23	Dark grey to black clay laid down in shallow standing water	
5.23	Stone	
Wied Żembaq 2:		
1.15–1.35	Alluvial brownish red clay	
1.35–5.07	Alluvial brown to dark grey fine sandy clay occasionally with fine limestone fragments	at 2.95 m: 1880–1630 cal. BC at 4.95 m: 3330–2920 cal. BC
5.07–5.13	Dark bluish grey sandy clay to clay	
Mġarr ix-Xini:		
0.54–2.43	Grey sandy silts and shelly sands: shallow marine sediments	at 1.76 m: AD 690–880
2.43–3.06	Grey clayey silts	
3.06–3.65	Laminated grey clay and sandy muds	
3.78–4.95	Alternating laminae of fine to coarse gravel with silt and silt/sandy muds	
4.95–5.72	Yellow/grey gravelly sandy muds	
5.72–6.21	Brownish black sandy silts	
6.45–6.8	Yellow sandy muds and gravels	
6.8–6.93	Muddy breccia	
6.93–7.12	Grey clay	
7.12–7.21	Coarse and fine sands	at 7.17 m: 1490–1290 cal. BC
7.21–7.43	Massive coarse and fine gravel	
Marsaxlokk 1:		
0.12–0.5	Calcitic fine sandy/silt loam topsoil	
0.5–2.92	Alluvial sandy/silts to silty clay loams interrupted by three lenses of fine gravel and coarse sand	at 0.86 m: cal. AD 420–560 at 1.86 m: 540–380 cal. BC at 2.86 m: cal. AD 440–670
2.92–3.86	Reddish brown calcitic silty clay loam: *in situ terra rossa* soil	
Marsa 2:		
0–1.2	Pale brown silt, probably eroded soil material as the topsoil	
1.2–1.7	Large boulder	
1.95–3.9	Pale grey sandy/silty clay	at 2.7 m: cal. AD 430–650
3.9–5.2	Laminated dark grey silty clay and sands	
5.2–6.4	Sands and gravels	at 5.98 m: 980–840 cal. BC
6.75–7.0	Boulder	
7.0–9.05	Yellowish brown coarse gravels with sand and silt interbeds	
9.05+	Limestone bedrock	
Mellieħa Bay:		
0.44–1.19	Mixed sand, clay and organic mud	(no dating for this core)
1.19–2.0	Fine-medium sands with hints of bedding	
2.0–5.14	Glauconitic coarse to medium sands, slowly fining upwards	
5.14–5.36	Humic sandy/silty clay with eel grass fragments	

below the wave-base. At 5.15 m this passes into glauconitic medium to coarse sands which generally fine upwards. These accumulated within the wave-base. The sands become slightly finer and exhibit hints of bedding 1.6–1.48 m below ground surface. These sediments are shallow marine lagoonal sediments, most probably deposited in *Posidonia* meadows. The upper 1.48 m exhibits alternating thin horizons of silty

clay, coarse-medium sand and black organic mud. These sediments relate to beach, dune, dune slack and marshland environments.

2.3.3. Magnetic susceptibility and XRF analyses of the cores

Charles French & Rory Flood

A selection of sediment cores was subject to digital core scanning for resistivity and magnetic susceptibility analyses as well as XRF (X-ray fluorescence spectrometry) multi-element analyses. These were undertaken at the Physical Geography Laboratory at University College Dublin and the Geography Department, NUI Maynooth, using an ITRAX XRF core scanner and a GEOTEK Multi-Sensor core logger. Example resistivity and magnetic susceptibility graphs for Xemxija cores 1 and 2 (Figs. 2.10 & 2.11) and multi-element graphs of results for the Xemxija 1 core as well as the Marsaxlokk and Wied Żembaq 1 cores are presented here (Figs. 2.4 & 2.12–2.14).

In both Xemxija cores, there is a remarkable high to low transition in magnetic susceptibility (MS) values that occurs at the level at which the palaeosol begins to become buried by alluvial deposits at a depth of *c*. 8/9 m below ground surface at some time before *c.* 4330–4050 cal. BC (Tables 2.3 & 2.4; Figs. 2.10 & 2.11). This remarkable step-change in high to much lower values may well reflect the change from a relatively stable, albeit probably slowly aggrading (with hillwash) buried soil of the earlier Holocene to a lengthy, later erosive phase above (see Chapter 5). Moreover, the relative troughs and peaks of MS values within the palaeosol itself, could well indicate several (at least four) phases of stable ground surfaces interspersed with phases of colluvial addition to this buried soil profile. For the remainder of the magnetic susceptibility curve upwards, especially in the Xemxija 1 core, the values remain lowish and constant, corroborating the absence of standstill phases in this valley fill sequence, except perhaps at *c*. 4.6 m or 2200–1980 cal. BC where paludal marsh deposits are overlain by renewed alluvial accumulation.

Most element values remain relatively constant throughout the whole depth of the cores (Figs. 2.12 & 2.13). There are, however, a number of exceptions to these trends in some elements. For example in Xemxija core 1, calcium (Ca) begins to increase and fluctuates in values from a depth of *c*. 6.5 m, and especially upwards from *c*. 4.6 m. This coincides with the continuing deposition of alluvial deposits (Table 2.4), and suggests greater disturbance, soil surface exposure and evapo-transpiration leading to the formation of secondary calcium carbonate in the soil/sediment complex as the seasonally alluviated profile dries out repeatedly (Durand *et al*. 2010). Phosphorus (P) is consistently moderately enhanced until the upper *c*. 4 m of the profile. This could reflect a reasonably steady input of plant material into the palaeosol and eroded/redeposited soil material (or alluvium) in the lower part of this core (Cook & Heizer 1965, 12ff; Holliday & Gartner 2007; Karkanas & Goldberg 2010; Linderholm & Lundberg 1994; Middleton & Price 1996; Wilson *et al*. 2005, 2009), a feature which distinctly lessens in the upper *c*. 4 m of the profile.

Potassium (K) in Xemxija core 1 shows distinctive decreases in values between 7.5 and 8 m, and at *c*. 6.5, 5.3–5, 3.9, 3.1, 2.5 and 1.5–1 m below ground surface. These phases more or less equate with phases of sediment influx associated with overbank flood deposits (Table 2.4), and could suggest variable inputs of plant nutrients (Fageria & Baligar 2005). Iron (Fe) is relatively more variable between *c*. 8.8 and 7 m, and is possibly indicative of the opening-up and disruption of the palaeosol. Sulphur (S) exhibits a larger range of more consistent peaks at *c*. 6.5–5 m, which could relate to slight changes in pH (or reduced alkalinity) related to organic inputs (Boreham *et al.* 2011). Arsenic (As), selenium (Se) and bromide (Br) all exhibit a distinctive peak at *c*. 5.25–5 m. Many elements decline or remain low but steady towards the top of the core, but strontium (Sr) becomes much more pronounced between *c*. 2.25–1.5 m, as do tin (Sn) and antimony (Sb) to a lesser extent. These increases may reflect modern soil pollutants (Declercq *et al*. 2019; Wilson *et al.* 2005, 2009).

In the Wied Żembaq 1 core (Fig. 2.13; Table 2.4), aluminium (Al), silica (Si), magnesium (Mg) and phosphours (P) remain constant throughout. These elements, along with iron (Fe) and potassium (K) which exhibit considerable variation, suggest a set of macro- and micro-nutrients inputs, plant matter and ash, reasonably advantageous to agriculture, into the valley system, possibly through phases of soil erosion from the wider valley catchment (Fageria & Baligar 2005). Calcium (Ca) increases between *c*. 5–4 m and markedly above *c*. 3 m, which again possibly suggests increasing evapo-transpiration and aridity (Durand *et al.* 2010). Strontium (Sr), tin (Sn) and antimony (Sb) increase sharply above 1.5 m, as at Xemxija 1, possibly relating to more recent pollution in the valley system (Declercq *et al*. 2019; Wilson *et al.* 2005, 2009).

In the Marsaxlokk 1 core, there is a much greater range of data and irregularities exhibited (Fig. 2.14; Table 2.4). There appears to be a major step-change just above *c*. 3 m in the plots for iron (Fe), potassium (K), managanese (Mn), rubidium (Rb), titanium (Ti), zirconium (Zr) and yttrium (Y). This could suggest a shift towards drier conditions, less input of eroded soil materials and less groundwater in the valley sediments.

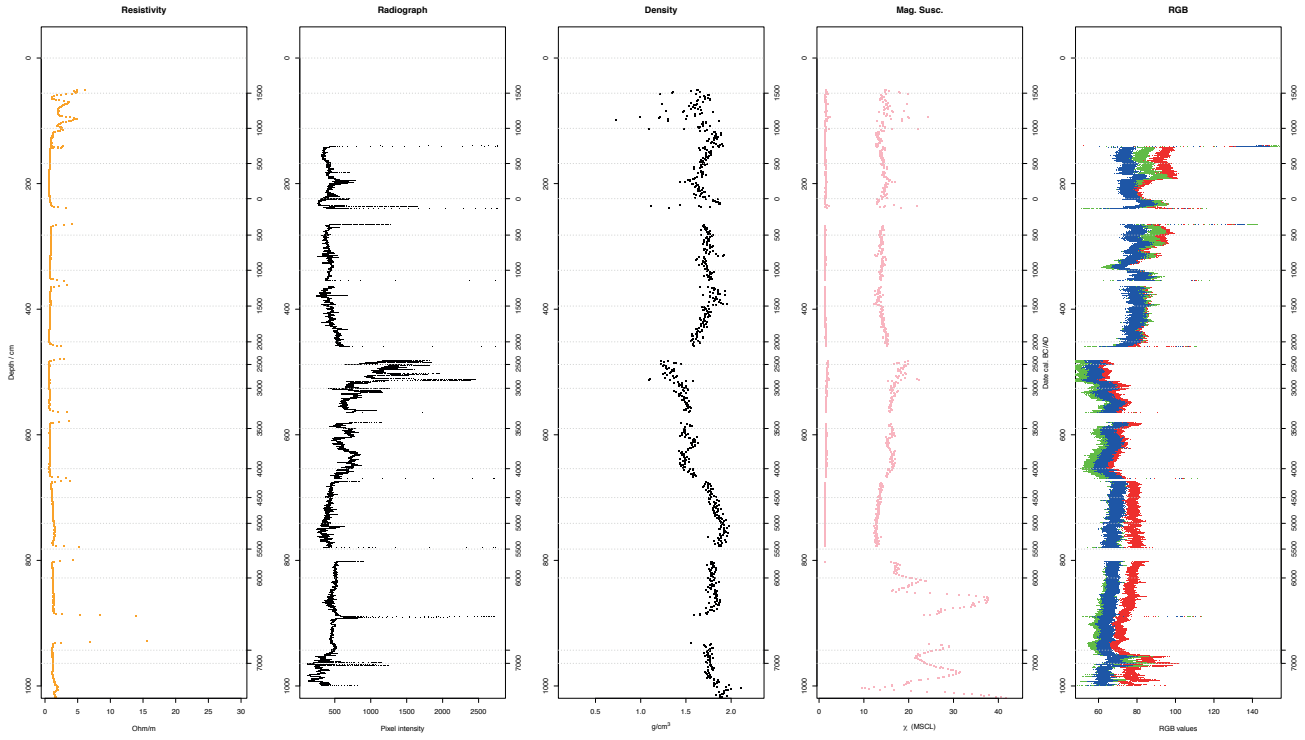

Figure 2.10. *The resistivity and magnetic susceptibility graphs for Xemxija 1 core (R. Flood).*

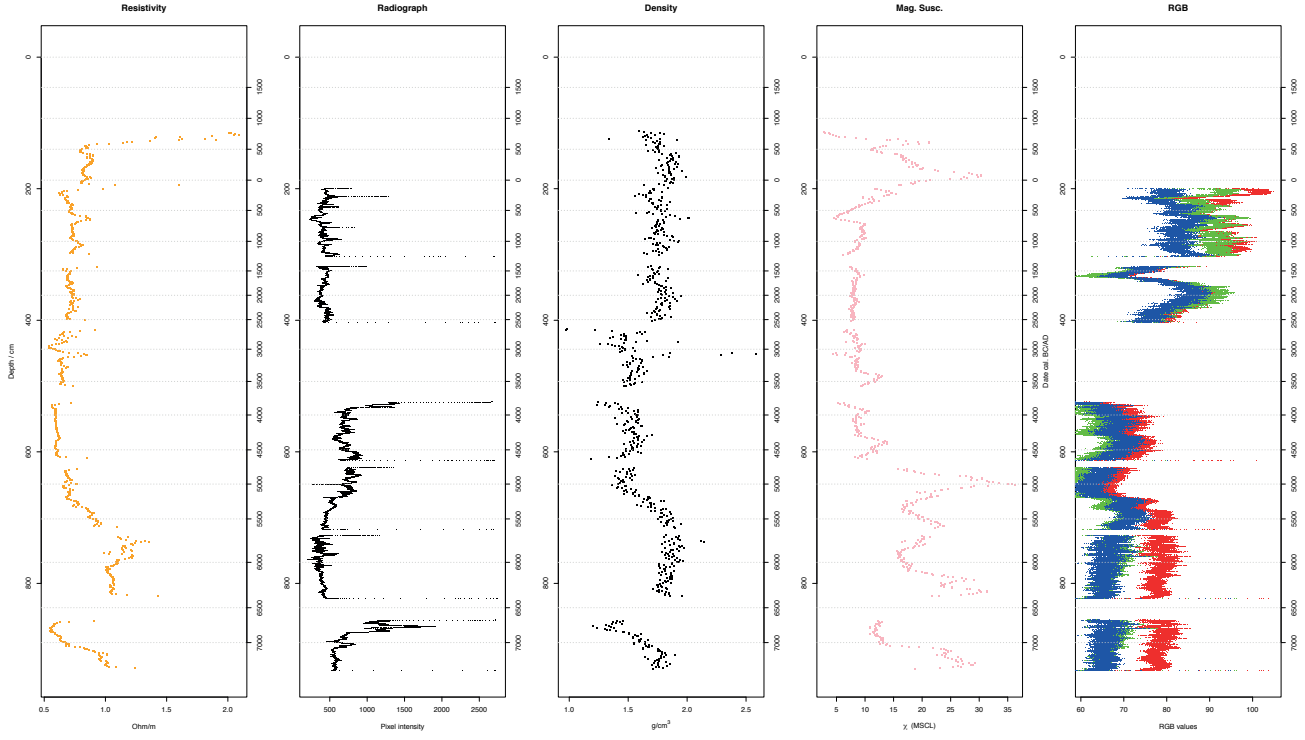

Figure 2.11. *The resistivity and magnetic susceptibility graphs for Xemxija 2 core (R. Flood).*

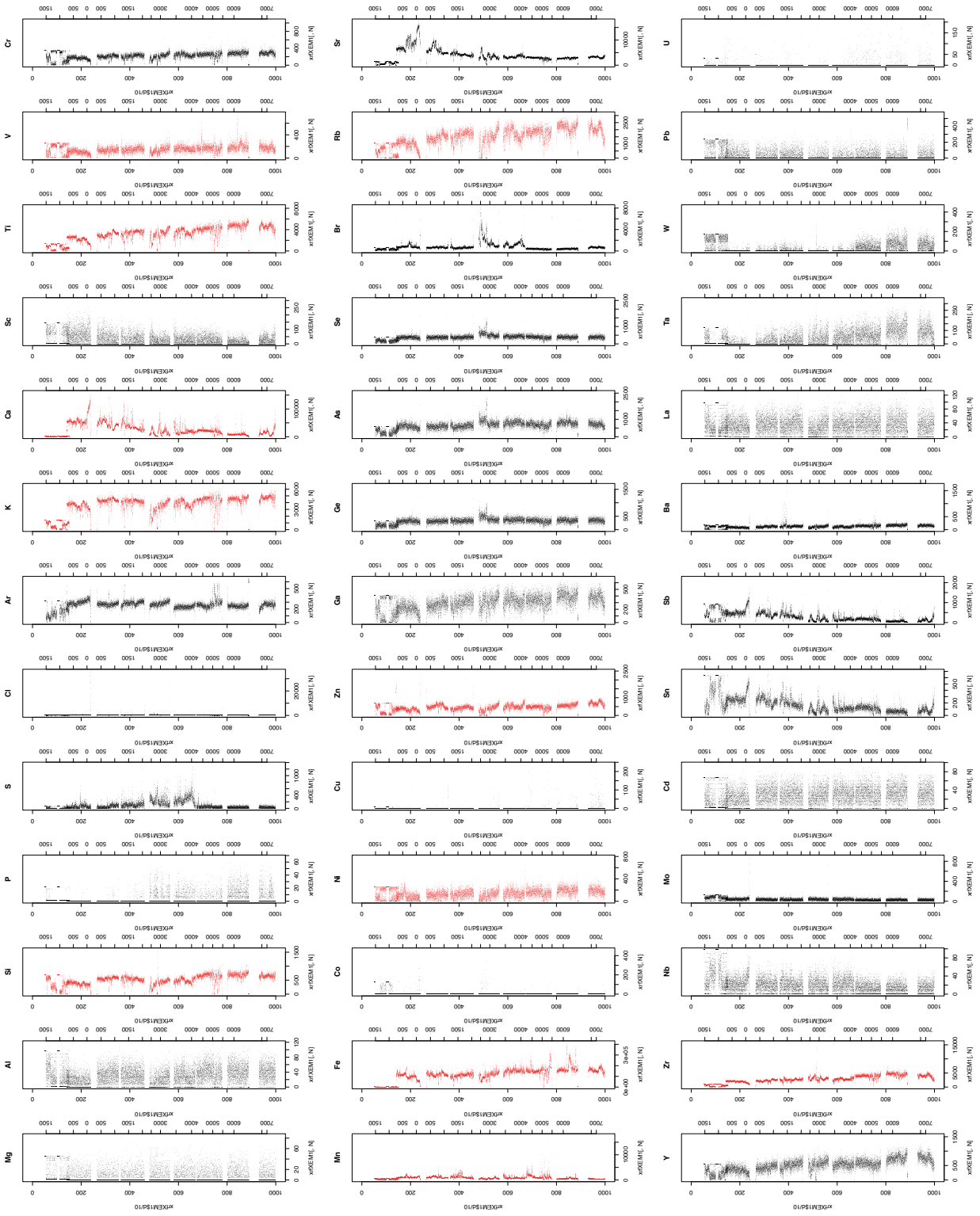

Figure 2.12. *The multi-element data plots for Xemxija 1 core (data from R. Flood, Steve McCarron & Jonathan Turner).*

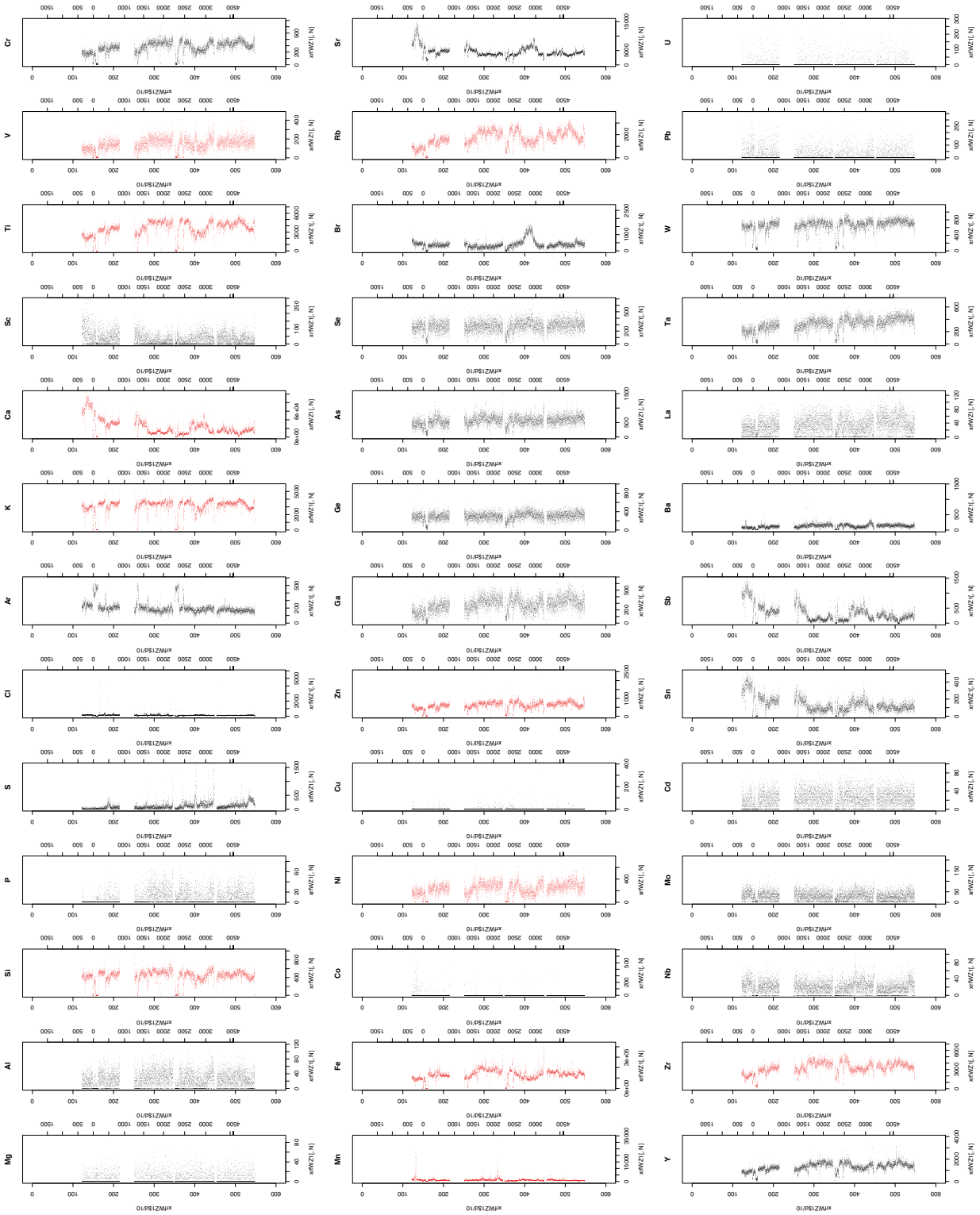

Figure 2.13. *The multi-element data plots for Wed Żembaq 1 core (data from R. Flood, Steve McCarron & Jonathan Turner).*

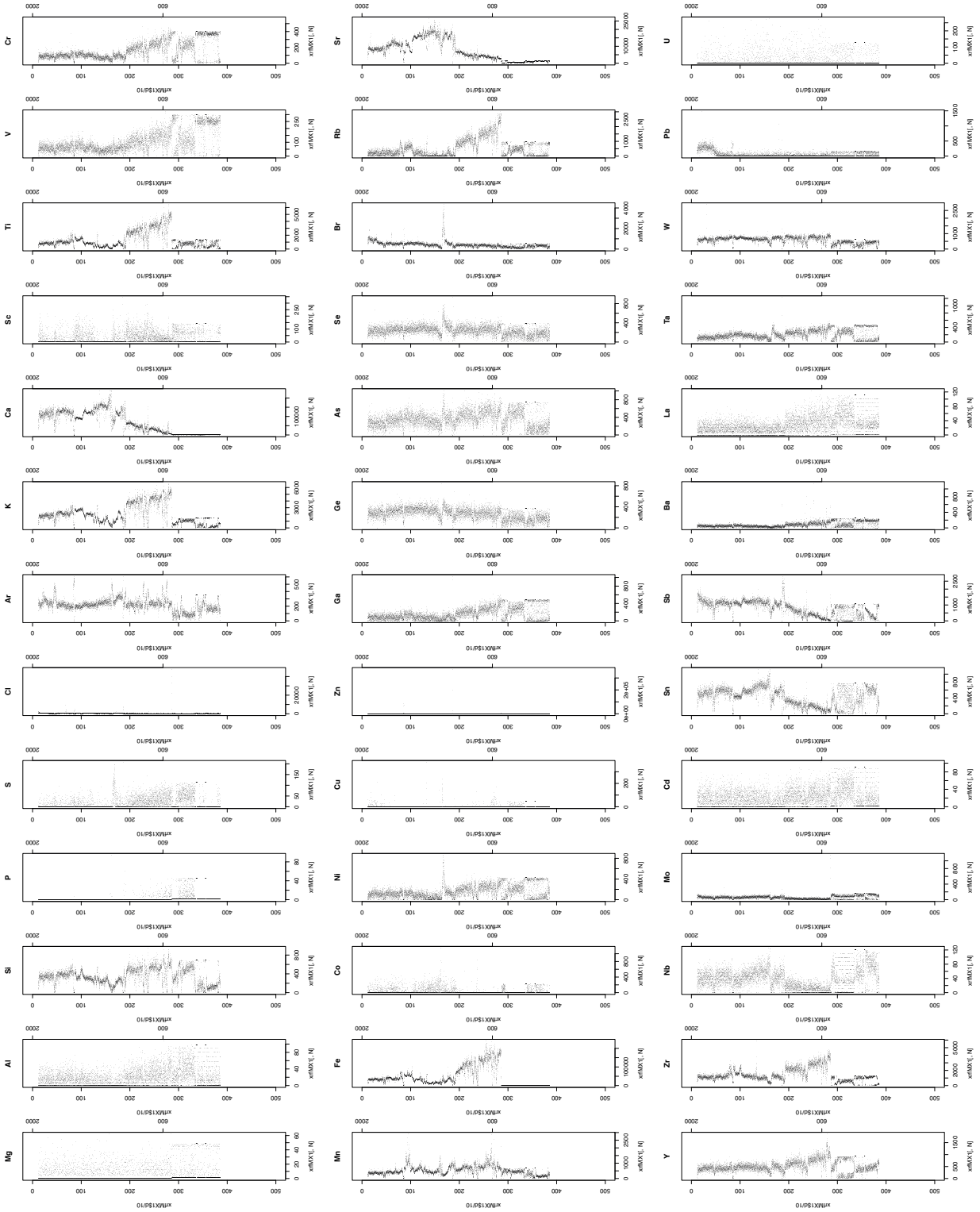

Figure 2.14. *The multi-element data plots for Marsaxlokk 1 core (data from R. Flood, Steve McCarron & Jonathan Turner).*

2.4. Age-depth models

Maarten Blauuw & Rowan McLaughlin

The chronology of each core was established using the data presented in Table 2.3, and then an age-depth model constructed as a statistical description of the relationship between time and the depth of burial of the sediment, and hence the age of the material enveloped within it (Table 2.5). Such models are calculated by first obtaining dates (usually but not necessarily radiocarbon dates) from multiple depths in the sediment profile, then extrapolating between these depths so that the age of any depth in the profile can be inferred. All but the simplest age-depth models are calculated using computers and numerous methods have been developed, including linear interpolation between the dated levels, or fitting a parametric model – a mathematical description of a changing sedimentation rate – to the data points (e.g. Blaauw 2010). More sophisticated approaches deploy various Bayesian methodologies that aim to build realistic chronologies and appropriately sized confidence intervals. This can be done through constraining the data with prior information about the gaps between the dated levels (Bronk Ramsey 2008a) or by modelling the sediment accumulation process itself (Blaauw & Christen 2011). In these cases, the shape of the age-depth curve is deduced through the analysis of millions of 'random walks' or random samples of the data, and is quite computationally intensive, even for the relatively fast computers available at the time of writing.

The age-depth models provide a 'best guess' point estimate for the age of any depth in sediment cores, and an associated confidence interval. For detailed study of certain palaeoecological events, the posterior probability distribution of the age for any given depth can also be extracted and analysed further. The *FRAGSUS Project* used *Bchron* (Parnell *et al*. 2008) and (primarily) *Bacon* (Blaauw & Christen 2011) to derive the age-depth models, using the data given in this chapter. Plots of the summed radiocarbon ages for the main sediment cores (Mġarr ix-Xini, Xemxija, Salina and Wied Żembaq) are given in Figure 2.2.

2.4.1. Accumulation rates

One advantage of the approach to sediment chronology advocated by Blaauw and Christen (2011) is that the sediment accumulation rate is modelled explicitly, and therefore robust estimates of it can be obtained, together with its uncertainty, and plotted as a function of time. This was done for each sediment core so that any synchronous changes in accumulation rate could be identified. Here, however, the confidence intervals of these estimates were quite large, although some useful general observations can be made. In the majority of the cores, the accumulation rate did not appear to change significantly from the confidence intervals of the modelled accumulation rates.

The mean sediment accumulation rate is a function of many factors including the underlying geology, topography, hypsometry, connectivity of drainage channels, catchment size, vegetation cover, soil properties and, in coastal locations, sea level (Table 2.5). None of these factors can be correlated with the mean accumulation rate and all change with time, so steady accumulation rates cannot be seen as evidence for stasis, but rather that the sedimentation within each catchment is driven by a set of variables whose evolving relationship leads to a relative stability when taking a long-term view. An exception to this is the Salina catchment, which according to the Salina Deep Core, experienced a slower accumulation of sediment at the coring site from around 4000 cal. BC, probably largely as a result of rising sea levels (see §3.6). The timing of this is interesting, as it roughly coincides with the start of the 'Temple Period' in Malta, and the intense phase of cultural activity that led to the construction and use of megalithic sites. Frustratingly this moment in time is represented by sediments near the top of the portion of the Salina Deep Core that was suitable for analysis, and at the bottom of the 10 m cores (Salina 3 & 4) retrieved from further inland.

Table 2.5. *Mean sediment accumulation rates per area versus time for the deep cores.*

Core	Period	Mean acc. rate (yr/cm)	Area (sq. km)	Hypometric index
Marsa 2	2000 BC–present	4.6	47.9	.41
Marsaxlokk	AD 100–present	9.5	0.6	.43
Mġarr ix-Xini	500 BC–present	3.6	4.5	.63
Salina 3 and 4	5000 BC–present	7	39.6	.45
Salina Deep Core	7500–4000 BC	2.5	39.6	.45
Salina Deep Core	4000 BC–present	4.3	39.6	.45
Wied Żembaq 1 and 2	3500 BC–present	11.1	11.0	.55
Xemxija 1 and 2	8000 BC–present	10.9	7.2	.41

Therefore, it has not been possible to refine the dating of this transition, as suitable samples for dating and modelling do not exist.

It must be stressed that the pictures provided by short-term and long-term sediment accumulations are radically different. In the cores, there is evidence for discontinuities and short phases of rapid sedimentation, as discussed below.

2.5. A local marine reservoir offset for Malta

Paula J. Reimer

Radiocarbon ages of organisms that lived in the ocean have an older apparent age than contemporaneous terrestrial organisms because of the long residence time of carbon in the ocean (Mangerud & Gulliksen 1975). This apparent age, or reservoir age R, is around 400 years on average throughout most of the Holocene, but age also depends on regional and local conditions such as upwelling of older carbon or input of freshwater from rivers. In order to convert radiocarbon ages to calendar year equivalents and to correct for this difference for marine organisms or humans and animals who consumed these, we need to estimate the local or regional offset, ΔR, from the global marine calibration curve (Stuiver *et al*. 1998). ΔR is usually evaluated by measuring known age corals or mollusc shells which grew prior to the increase in radiocarbon (^{14}C) in the atmosphere because of nuclear weapons testing ('bomb' carbon) or accessing 'pre-bomb' values from the Marine Radiocarbon Reservoir Correction Database (Reimer & Reimer 2001; www.calib.org). There are currently no published measurements from 'pre-bomb' mollusc shells near Malta, since the closest results came from the north of Sicily. It was therefore necessary to determine ΔR from marine mollusc shells collected near Malta in order to be able to properly calibrate radiocarbon ages from marine samples for the *FRAGSUS Project*.

Two specimens of the filter-feeding cockle *Acanthocardia paucicostata* (both valves present) were obtained from the National Museum of Natural History, Malta, in order to evaluate ΔR for the region. These were originally collected live in the period 1914–19 (no exact date) by a well-known local naturalist, Giuseppe Despott, whose collection is held in the Museum. Both specimens come from the same locality, which is the area of the harbours in Valletta, very likely the Grand Harbour.

The shells were pre-treated with 1 per cent HCl to remove approximately 25 per cent of the mass, hydrolysed to CO_2 using phosphoric acid (H_3PO_4) and converted to graphite using the hydrogen reduction method (Vogel *et al.* 1984). The $^{14}C/^{12}C$ ratio of the graphite was measured using accelerator mass spectrometry (AMS). The $^{14}C/^{12}C$ ratio was background corrected, normalized to the HOXII standard (SRM 4990C; National Institute of Standards and Technology) and corrected for isotopic fractionation using the AMS-measured $\delta^{13}C$ which accounts for both natural and machine fractionation. The ^{14}C age and one standard deviation were calculated using the Libby half-life (5568 years) following the conventions of Stuiver and Polach (1977). The ΔR values were calculated from the difference in the measured radiocarbon age of the shells and the radiocarbon age of the marine calibration curve, Marine13 (Reimer *et al*. 2013) using the programme *deltar* (Reimer & Reimer 2017) (Table 2.6).

Table 2.6. *Radiocarbon measurements and ΔR values from early twentieth century ('pre-bomb') marine shells from Malta.*

Lab number	Museum ID	^{14}C date yrs BP	ΔR ^{14}C yrs
UBA-31424	MNH/CON 01326	406±24	-42±24
UBA-31425	MNH/CON 01326	593±24	144±24

There is a statistically significant difference in the radiocarbon ages and ΔR values for these two samples so the values cannot be averaged. Therefore we calculate a weighted mean ΔR and used the square root of the variance to determine the uncertainty which yields a ΔR for Malta of 51±93 ^{14}C years.

A single measurement from Sicily of *Cerastoderma corrugatum* collected in 1900 (Siani *et al*. 2000) provides a comparison value of 71±50 ^{14}C years when calculated with the Marine13 calibration curve (Reimer *et al*. 2013). This value is in agreement with the mean ΔR for the two Malta shells.

The difference in the ΔR values for the two Maltese samples is possibly a consequence of proximity to freshwater input into the harbour. Freshwater from regions of ancient limestone such as Malta can increase ΔR because the dissolved carbonate contains no radiocarbon. Without further analyses on a number of additional samples, any marine radiocarbon samples from Malta will therefore have rather large calibrated age ranges. To improve the ΔR value for Malta, more known age, 'pre-bomb' samples, preferably from locations without freshwater input, would need to be analysed.

2.6. Major soil erosion phases

Rory P. Flood, Rowan McLaughlin & Michelle Farrell

2.6.1. Introduction

Although erosion is an important part of the sedimentation process that leads to the accumulation of deposits suitable for palaeoenvironmental study, severe erosion is problematic in that parts of the sequence can be removed entirely, creating an 'hiatus',

and the upstream mixing of bulk materials may lead to much recycling of older carbon. As a result of these processes, the radiocarbon samples from Maltese sequences were, on occasion, unintentionally procured from materials much older than the sediments in which they were buried. The timing of these episodes of erosion is nonetheless important, and indeed pertinent to the *FRAGSUS Project*'s attempts to understand better the role that environmental changes had in shaping social progress and vice-versa. Two methods were used to estimate the timing of erosion events; statistical analysis of errant 'old' dates from the sediment cores, and new OSL dates obtained from valley fills (see §2.1.1.3). As discussed below and in Chapter 5, soil erosion is an important factor in the evolution of Mediterranean landscapes generally, and in Malta and Gozo especially. Many direct indicators of erosion are present in the cores, such as the sedimentology (see §2.3.2) or the presence of certain biota, especially root fungal symbionts and burrowing snails which were transported from areas of eroding soils into aquatic deposition sites (see Chapter 4).

Soil erosion leading to the thinning of soil on hillslopes and thickening in valley bottoms, and associated changes in soil properties, is generally considered to be the primary vector in Mediterranean landscape evolution during the Holocene (Judson 1963; Vita-Finzi 1969; Hughes & Thirgood, 1982; Bintliff 1992; Butzer 2005; Dusar *et al*. 2011). Mediterranean environments have high rainfall intensities, alternating between wet and dry periods but with low average annual precipitation, and inherently fragile, slowly developing soils, low in nutrients and organic matter (García-Ruiz & Lana-Renault 2011; García-Ruiz *et al*. 2013). Coupled with a predominance of steep slopes and a long history of deforestation, natural fires, and cultivation in extreme topographic situations, these factors have led to extensive soil loss (Wainwright & Thornes 2004; García-Ruiz *et al*. 2013; Dotterweich *et al*. 2013). Geomorphological, pedological, palaeoecological, and geoarchaeological studies have detected significant soil erosion events dating from the Bronze Age and later throughout Mediterranean Europe (Dotterweich 2008), for example in Greece (Van Andel *et al.* 1998; Lespez 2003; Fuchs *et al.* 2004; Bintliff 2005), Cyprus (Fall *et al.* 2012), Turkey (Brückner *et al*. 2005), Italy (Marchetti 2002; Eppes *et al.* 2008; Piccarreta *et al*. 2011, 2012; Pelle *et al*. 2013), southwestern France (Bertran 2004) and Spain (Cerdá 2008; García-Ruiz 2010).

The Maltese Islands contain rich archaeological evidence for the presence of successive human societies, who were present by at least *c*. 5400 cal. BC, with a Neolithic fluorescence occurring around 3400–3000 cal. BC involving the construction of megalithic 'temples' and elaborate funerary hypogea (Evans 1971; Malone *et al*. 2009a; Pace 2000; Zammit 1928a; 1930). Based on palynological data from Burmarrad in northwest Malta (Djamali *et al*. 2013), Salina Bay in northwest Malta, Marsa in southeast Malta and Santa Marija Bay on the island of Comino (Carroll *et al.* 2012), and the archaeological site of Tas-Silġ (Hunt 2015), it appears that the Neolithic and later land-cover of the Maltese Islands largely comprised agriculturally degraded steppe and garrigue communities (see Chapter 3). Little, however, has until recently (see Malone *et al.* in press and this volume) been known about the intensity and extent of prehistoric subsistence agriculture in Malta, beyond the presence of typical 'Neolithic package' cultivars such as wheat, barley and legumes, and domestic livestock (Trump 1966; Renfrew 1972). In particular, it is not clear whether the prehistoric inhabitants of Malta took steps to mitigate the effects of soil erosion. This study investigates this problem in combination with the molluscan and palaeosol data presented in the following Chapters 3–5.

2.6.2. Methods

A combination of methods including AMS dating and sedimentology of the deep cores, hypsometry, and the application of the revised universal soil loss equation (RUSLE) were used in this soil erosion study. Eight sedimentary cores were recovered from four locations on Malta (Marsa, Xemxija, Salina and Wied Żembaq) and one from Gozo (Mġarr ix-Xini) (see §2.3.2) (Fig. 2.4). The Marsa sequence was previously studied by Carroll *et al.* (2012) and Fenech (2007) and all other sequences were investigated as part of this project. Radiocarbon dating of material from the sediment cores and the buried soils associated with the Santa Verna, Ġgantija and Skorba temple sites was performed at the ^{14}CHRONO centre, Queen's University Belfast, using accelerator mass spectrometry (AMS) (Tables 2.3 & 2.7). Previously published radiocarbon dates were also utilized (Carroll *et al*. 2012; Djamali *et al*. 2013; Marriner *et al*. 2012). The dates were calibrated using the IntCal13 and Marine13 calibration curves as appropriate (Reimer *et al*. 2013) and the resulting probability distributions were summed (Williams 2012) for dates that appeared out-of-sequence relative to their order in the core. In this way, the radiocarbon record can be interpreted as a potential indicator of carbon burial rate and erosion intensity (Long *et al.* 2016, 588).

Hypsometry is a measure of the relative proportions of land at different elevations (Strahler 1952). The hypsometric curve represents the relative proportion of land below (or above) a given height and together with the hypsometric index (HI), or elevation/relief ratio, can be used as an indicator of the geomorphic

form of a given catchment and its stage of evolution (Strahler 1952; Lifton & Chase 1992; Chen *et al*. 2003; Willgoose & Hancock 1998). Differences in the shape of the hypsometric curve and hypsometric index (HI) for landforms are considered to be related to the degree of disequilibrium in the balance of erosive and tectonic forces (Strahler 1952; Luo 1998; Weissel *et al*. 1994). Hence HI is often employed to explain erosion and/or sediment dynamics as catchments which are more recently incised possess high HI values, whereas catchments that have evolved into a lower dynamic equilibrium have lower HI values and in turn, smaller sediment yields (Wyatt 1993; Willgoose & Hancock 1998; Haregeweyn *et al*. 2008). The Maltese Islands were delineated in ArcGIS 10.1 from a 1 m resolution digital terrain model derived from airborne LiDAR last return data, with the outline of drainage basins established using standard tools in ArcGIS. Hypsometric and HI analysis for each catchment within which a sediment core was collected was carried out using CalHypso (Pérez-Peña *et al*. 2009).

The revised universal soil loss equation (RUSLE) is a soil erosion model that estimates average long-term soil loss through sheet and rill erosion (Wischmeier & Smith 1978; Renard *et al.* 1997) (Fig. 2.15). It is the product of five factors: R, a measure of rainfall; C, a measure of ground cover; K, a measure of the intrinsic erodibility of the soil; LS, computed from slope length and steepness; and P, derived from management practice (Renard *et al.* 1997; Renschler & Harbor 2002). Although a RUSLE model for Europe has become available recently (Panagos *et al.* 2015c) its 100 m resolution lacks the necessary detail for studying the nature of relatively small Maltese catchments. A separate RUSLE model for Malta has recently been published (Sultana 2015), but in the present study it was considered that the potential for soil erosion in the islands is likely to be highly seasonally variable because of seasonal differences in rainfall (R factor) and ground cover (C factor) (Fig. 2.16) (and see Chapter 8). Therefore, new seasonal models were derived as a product of what follows.

The seasonality in rainfall is a key point when considering its erosive potential. In Malta rain in the summer months is rare, but heavy rainfall can occur during autumn, winter and spring (Mitchell & Dewdney 1961). High resolution rainfall data are not currently available for Malta, so to take account of seasonal variations in rainfall in the RUSLE model, the R-factor estimate of 1672.4 MJ mm/ha/h/yr of Panagos *et al.* (2015a) was used and converted to monthly values using the proportional contribution of monthly rainfall to an annual total of 603 mm (data obtained from www.maltaweather.com, accessed March 2016) (Fig. 2.16).

C-factors were calculated using the Normalized Difference Vegetation Index (NDVI) as an indication of relative biomass (Fig. 2.16). This is calculated from the amounts of visible and near-infrared light reflected by vegetation, and is therefore derivable from multi-spectral remotely sensed images (Tucker 1979). NDVI of 0 is indicative of non-vegetated land, 0–0.3 indicates moderate vegetation cover, and 0.3–1 indicates dense vegetation cover (Carlson & Ripley 1997). Multi-spectral LANDSAT 8 images of Malta were obtained from the United States Geological Service Earth Explorer (earthexplorer.usgs.gov, accessed November 2015), corrected for sun elevation and sensor response to top-of-atmosphere reflectance (Shepherd & Dymond 2003) and masked to exclude urban areas, since these are much more extensive now than in the past. These images were used to calculate rasterized NDVI surfaces for six dates during the years 2014 and 2015. The choice of date was based on the availability of cloud-free imagery for Malta in the LANDSAT 8 archives. Palynological data (see Chapter 3) indicate that the present seasonal and spatial patterns of the Maltese vegetation can be considered as a reasonably close approximation of past land-cover.

To derive the C factor used in this study, the NDVI surface was scaled by the equation given by (Van Der Knijff *et al*. 2000)

$$C = e^{-2\frac{N}{1-N}}$$

where N is the NDVI raster.

Using ArcGIS 10.1, K-factor rasters were derived from the results of MALSIS, the Maltese Soil Information System Project (Vella 2001; Sultana 2015) using Kriging. The LS factor raster was provided by the European Soil Data Centre (Panagos *et al*. 2015b). For the purposes of this analysis, the P-factor was held at 1.0, as the nature and spatial extent of this variable in the past is currently under investigation.

2.6.3. Results

2.6.3.1. Early Neolithic agriculture

The palaeosol investigated beneath the floors of Santa Verna temple is indicative of a stable, well drained and organized, clay-enriched (or Bt) horizon (see Chapter 5). The total organic fraction of this buried soil was measured via loss-on-ignition as 7.1 per cent. The charred plant remains it contained were dominated by domesticated barley, *Hordeum* spp. (n=8), but also included domesticates *Triticum aestivum/durum* (n=2, free threshing wheat), 33 other fragments of domesticated cereals, *Lens culinaris* (n=2, lentil), wild grasses (n=4),

Table 2.7. *Calibrated AMS ^{14}C dates of charred plant remains from Santa Verna palaeosol, Gozo.*

Laboratory code	Radiocarbon date BP	Plant taxon	Calibrated date span (yrs cal. BP/BC, 95% confidence)
UBA-31042	6412±44	*Triticum* cf. *dicoccum*	7424–7270 / 5474–5320
UBA-31043	6181±40	*Hordeum* (cf. hulled straight)	7236–6953 / 5286–5003
UBA-31044	6239±37	Fabaceae	7259–7019 / 5309–5069

wild vetch (n=3) and other unidentifiable fragments. Three AMS radiocarbon dates were obtained from this material to establish a secure time frame for arable cultivation of about 5474–5003 cal. BC (7424–6953 cal. BP; UBA-31042/3/4), and in all likelihood somewhat earlier (Table 2.7). The palaeosol also contained pottery sherds characteristic of the 'Għar Dalam' and 'Skorba' types. These radiocarbon dates therefore also establish a date range for these cultural styles in Malta, refining previous work (Trump 1966; Renfrew 1972). Importantly these dates generally agree with Carroll *et al.*'s (2012) estimate of 5500 cal. BC for the earliest beginnings of agriculture in Malta based on palaeoenvironmental evidence.

2.6.3.2. Sedimentary chronology

Radiocarbon dates from the sediment cores are presented in Table 2.3, showing some samples that are anomalously old relative to their position in the core. Under the premise that these samples were originally enveloped within sediment during episodes of heightened sediment flux in each catchment, the distribution of their radiocarbon ages is thus a proxy for past landscape instability. A comparison of these out of sequence radiocarbon dates with those that appear to be in the correct sequence (Fig. 2.2) indicates that considerable parts of some sediment profiles contain material of mixed ages. The most prominent episode (of recycling of older material?) spans 1500 to 850 cal. BC, which broadly coincides with the Borġ in-Nadur phase of the Maltese Bronze Age.

2.6.3.3. Hypsometry

The hypsometric indices and other physical properties of the drainage basins under study are shown in Table 2.8. The data show that in Malta HI appears to be independent of catchment size, in contrast to the findings of Verstraeten and Poesen (2001) for small intensively cultivated catchments in central Belgium. Instead, at Xemxija, Salina, and Marsa, the HI values are very similar but catchment sizes vary between 7.2 sq. km and 47.9 sq. km (Table 2.7). In the cases of the Mġarr ix-Xini and Wied Żembaq catchments, coupling the HI values of 0.5–0.6 with the associated hypsometric curves demonstrates that both catchments are more susceptible to erosional processes. The data indicate that the Xemxija, Marsa, and Salina catchments are susceptible to fluvial erosion, whereas the Mġarr ix-Xini and Wied Żembaq basins show a greater susceptibility to hillslope processes such as landslides and debris flows (Strahler 1952; Wyatt 1993; Willgoose & Hancock 1998; Verstraeten & Poesen 2001; Haregeweyn *et al*. 2008).

2.6.3.4. Seasonality

Mean NDVI values on a selection of days in 2014–15 are shown for each catchment in Table 2.9. The choice of date was based on the availability of cloud-free imagery for Malta in the Landsat 8 archives.

2.6.3.5. RUSLE model of present-day erosion potential

Resulting RUSLE surfaces for September and March are shown in Figure 2.15 (and see Chapter 8, Fig. 8.2), with R (rainfall-runoff) and C (cover) values being strongly time dependent. The product of R and C models the seasonal signal in soil erosion (Fig. 2.16) which, holding other factors constant, indicates that the potential for soil erosion in Malta from mid-September to mid-December is much higher than at other times of the year.

2.6.4. Discussion

The soils of the Maltese Islands are inherently and easily erodible because of relatively sparse vegetation cover, intensive rainfall during storms, the commonly very fine sand and silt dominated soil fabrics, and a

Table 2.8. *Physical properties of the catchments.*

Catchment	Area / sq. km	Hypsometric Index	Hypsometric interpretation (cf. Willgoose and Hancock, 1998)	Mean LS Factor
Mġarr ix-Xini	4.50	.63	Unstable	1.09
Xemxija	7.23	.41	Fluvial erosion	1.77
Salina	39.66	.45	Fluvial erosion	1.17
Marsa	47.92	.41	Fluvial erosion	.86
Wied Żembaq	11.04	.55	Hillslope processes	.54

Table 2.9. *Normalized Diffuse Vegetation Index (NDVI) for the catchments in 2014–15 and average rainfall data for the weather station at Balzan for the period 1985 to 2012.*

Catchment	NDVI					
	January	March	June	September	November	December
Mġarr ix-Xini	.54	.55	.23	.22	.31	.38
Xemxija	.49	.55	.33	.29	.40	.46
Salina	.47	.57	.31	.25	.40	.48
Marsa	.53	.56	.29	.25	.36	.44
Wied Żembaq	.51	.55	.26	.25	.38	.44
Mean rainfall (mm)	94.7	37	5.4	67.4	108.6	107.7
R-factor (MJ mm (ha hr month)$^{-1}$	263	103	15	187	301	299

relatively large proportion of elevated land. Today, erosion is most likely to occur between September and December each year, and such episodes that have occurred in the recent past have led to the formation of several metres of sediment accumulation on basin floors. For example, a three-day stormy episode in October 1957 led to the removal of 25 mm of topsoil from land surfaces via sheet erosion, walls built across valley floors were swept away, and gullies up to 1.2 m deep were formed, even in very small

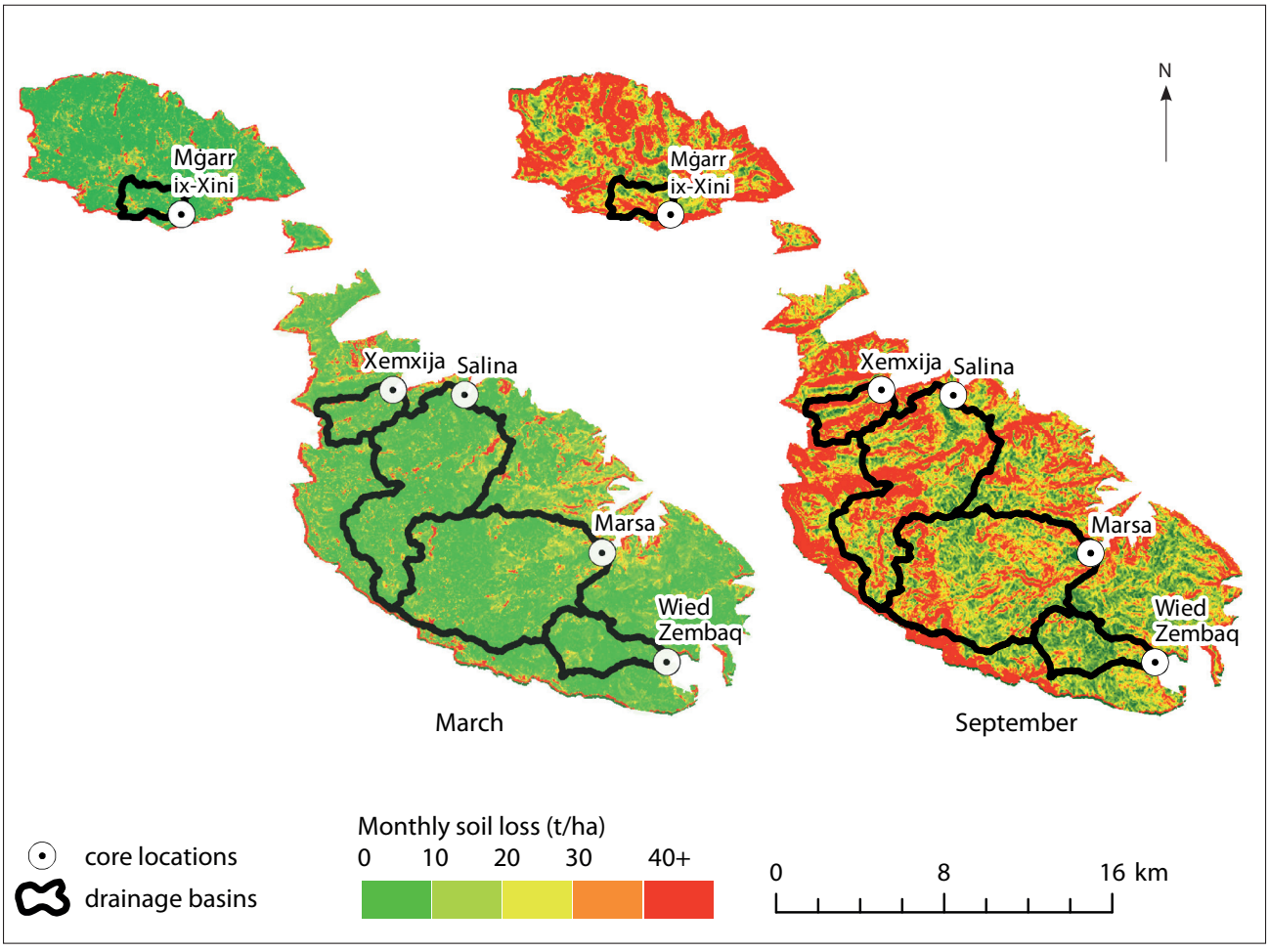

Figure 2.15. *RUSLE models of soil erosion for the Maltese Islands in September and March (R. McLaughlin).*

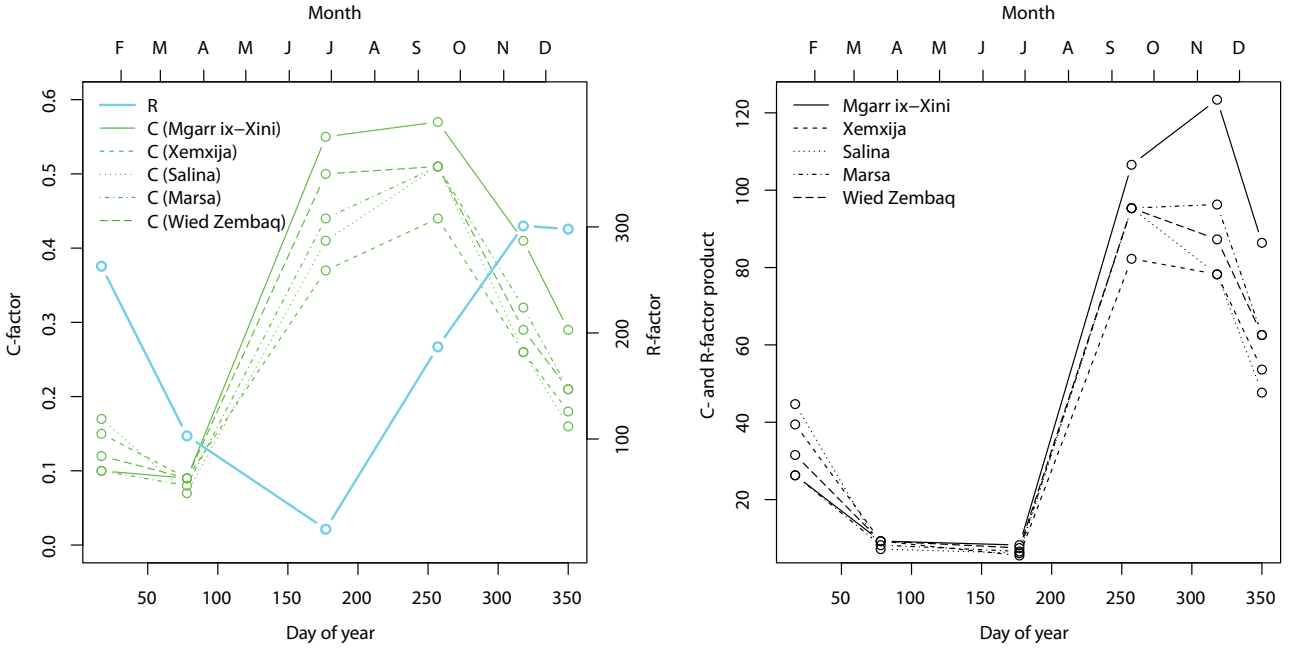

Figure 2.16. *R and C factors and their product (R. McLaughlin).*

catchments (Mitchell & Dewdney 1961). Such events are not atypical, indeed up to 40 per cent of rainfall in Malta occurs during the six wettest days of the year (Mayes 2001). Heavy rainfall is markedly regional, both within any one storm and overall. Some areas seem more susceptible to heavy rainfall than others, with flat land areas draining a large catchment suffering badly from erosion (Mayes 2001; Mitchell & Dewdney 1961).

Although the potential for sudden, catastrophic soil loss is high, the seasonal cadence of Maltese soil erosion events renders them predictable, and agricultural practices and social management can be adapted accordingly (see Chapter 8). Precisely how these management strategies were enacted during prehistoric times is not forthcoming from the archaeological record, although the long sequences of deposits found in the valley floors offer some hints that the strategies changed with time, and occasionally failed altogether.

The inherent fragility and instability of the Maltese landscape implies that agriculture there has always been at risk from soil erosion. The buried soil from Santa Verna indicates that the earliest phases of agriculture were associated with a rich, moist, vegetated soil (see Chapter 5), probably much more resistant to erosion than the soils present in Malta today. Accumulation of sediment in valleys during this time indicates that the steps taken to prevent erosion were limited. During the 'Temple Period' from about 3900 cal. BC, archaeological evidence indicates that cereals were grown and livestock raised, with increasingly elaborate cultural developments taking place at the same time (Fiorentino *et al.* 2012; Evans 1971; Trump 1966; Volume 2). Could this have been possible without a strategy for mitigating the effects of erosion? Although there is no direct archaeological evidence, whether the Temple Period landscape was terraced and whether there was a 'collapse' of the temple civilization at around 2350 cal. BC is a matter for debate. These issues are returned to in Chapters 5, 6 and 11, but what can be said is that there is no evidence of catastrophic destabilization in the valley sedimentary records during the later Neolithic period. However, a period of complete abandonment may be less visible in the sedimentary record because of natural stabilization caused by vegetation regrowth, and the relative lack of organic material in the cored deposits made those core sections difficult to date directly using radiocarbon methods.

The main period of landscape destabilization that is evident in the sediments studied here occurs much later, between *c.* 1550 and 1000 cal. BC during the 'Borġ in-Nadur' period. This time frame saw significant changes in settlement patterns on Malta, compared with previous periods, with the construction of defended settlements on prominent locations (Tanasi & Vella 2015) (see Chapter 7). This time is also one likely date of the 'cart-ruts' – widespread rock-cut tracks leading from hill-tops to valley bottoms. The morphology of these suggest previous soil cover on

hill tops now denuded of soil (Mottershead *et al*. 2010), and one possible explanation for their existence is the act of drawing soil uphill for agricultural purposes, so that food could be grown near the defended settlements, rather than in valley bottoms as is the case today (cf. Evans 1971, 203; Zammit 1928b). This soil management practice differed from soil management practices in the Neolithic and Temple periods for any number of societal reasons, but led to the loss of more soil than before.

It seems that the Phoenician settlement of Malta and Gozo, occurring in the eighth century cal. BC (Vella & Anastasi 2019), heralded a period of relatively greater stability for Maltese sediments which continued into classical times, but erosion was still continuing. Widespread olive and vine cultivation would have been an important factor in this continuing erosion story. It was a risky strategy as these practices typically leave the soil bare and loose and lead to increased soil erosion unless the vines are grown together with an understory of vegetation (Loughran *et al*. 2000; Kosmas *et al.* 1997). Archaeological traces of Phoenician-Punic and Roman olive cultivation and viticulture are widespread in Malta and Gozo (Vella *et al*. 2017; Anastasi & Vella 2018). Similar evidence is present in the environmental record; an increase in *Olea* pollen from *c*. 400 BC into the early Roman period (*c*. cal. AD 20–260) has been observed at Burmarrad (Gambin *et al*. 2016) and in the Marsa cores (see Chapter 3). The risk of disaster could be mitigated by food imports, as Malta was no longer economically self-sufficient during Phoenician-Punic and Roman periods (Bonanno 1990). However, the potential for soil erosion to lead to loss of crops and subsequent economic stress would have been high. Although there is no direct archaeological evidence, the RUSLE model combined with the archaeological and environmental evidence strongly suggest that terracing – or another landscape approach at least as effective as terracing, such as careful management of crop understories, was introduced or reintroduced shortly after *c*. 1000 cal. BC as a means to help control soil erosion.

2.6.5. Conclusions

In this study, it has been demonstrated that the catchments in Malta are a mix of unstable and more mature landforms with the best palaeoenvironmental sequences coming from small catchments with low hypsometric index (HI) values. Thus although there is a high potential for erosion in the Maltese Islands during winter months, the sedimentary history of the islands is punctuated by episodes of stability in the rest of the year. Agriculture was present in Malta from at least *c*. 5400 cal. BC, but varied in intensity throughout prehistory.

Soil erosion management is the key factor that links these issues (and see Chapters 5 & 8). Successive cultural developments took place from at least 5400 cal. BC onwards and the island's sedimentary histories demonstrate how the physical properties of soil and the underlying landforms exist in a system linked to social, economic and cultural factors. This system appears to be at constant risk of failure, leading to widespread soil erosion. Today, in regions isolated from global trade networks (e.g. Haggard *et al.* 2009), or in regions undergoing unchecked agricultural expansion (e.g. Yan *et al.* 2009), the potential of soil erosion to lead to a human cost is high (Bringezu *et al.* 2014). The history of other regions is also relevant in this respect. For example, Boyle *et al*. (2011) have described the 40-fold increase in soil erosion that followed agricultural expansion in early nineteenth century California, demonstrating that USLE-based soil erosion models could predict the phenomenon closely. Similarly, we present these seasonal RUSLE models in the hope that they will be useful in Malta for the on-going evaluation of soil erosion risk, conservation and management. A wider point is to emphasize the prominent role that managing soil erosion had in the day-to-day lives of people in the Mediterranean. From later prehistory onwards, the Mediterranean was the epicentre of many cultural, economic and technological advances, all of which were predicated on sustainable subsistence agriculture. As our Maltese case study illustrates, in such a setting, soil erosion presented an obstacle that could be overcome, but sometimes in concert with other changes in land use, led to a degradation of resources and likely stress.